Supplementary file

Reactive transport modeling of water-CO_2-rock interactions in clay-coated sandstones and implications for CO_2 storage

Huan Li[1], Qinhong Hu[2,*], Rukai Zhu[3], Bo Liu[3], Achyut Mishra[4], Eric O. Ansah[5]

[1] *Hubei Key Laboratory of Complex Shale Oil and Gas Geology and Development in Southern China, Yangtze University, Wuhan 430100, P. R. China*

[2] *National Key Laboratory of Deep Oil and Gas, China University of Petroleum (East China), Qingdao 266580, P. R. China*

[3] *Xinjiang Research Institute of Huairou Laboratory, Urumqi 830000, P. R. China*

[4] *Department of Earth Sciences, Indian Institute of Technology Gandhinagar, Palaj, Gandhinagar, Gujarat 382355, India*

[5] *WH Bryan Mining & Geology Research Centre, Sustainable Minerals Institute, University of Queensland, Brisbane 4072, Australia*

E-mail address: lihuantry@yangtzeu.edu.cn (H. Li); huqinhong@upc.edu.cn (Q. Hu); zrk@petrochina.com.cn (R. Zhu); liubo@nepu.edu.cn (B. Liu); achyut.mishra@iitgn.ac.in (A. Mishra); e.oansah@uq.edu.au (E. O. Ansah).

[*] Corresponding author (ORCID: 0000-0002-4782-319X (Q. Hu))

Li, H., Hu, Q., Zhu, R., Liu, B., Mishara, A., Ansah, E. O. Reactive transport modeling of water-CO_2-rock interactions in clay-coated sandstones and implications for CO_2 storage. Advances in Geo-Energy Research, 2025, 17(2): 121-134.

The link to this file is: https://doi.org/10.46690/ager.2025.08.04

1. Supplementary tables

Table S1. Kinetic parameters employed for solving mineral dissolution and precipitation rate laws.

Mineral	Chemical formula	Acid mechanism			Neutral mechanism		Base mechanism			*SSA*[a] (cm^2/g)	*ESA*[a] (cm^2/g)	Nucleus density (cm^2/cm^3)
		$k_{25\,℃}$[a] ($mol/cm^2/s$)	E_a[a] (kJ/mol)	n[a] (H^+)	$k_{25\,℃}$ ($mol/cm^2/s$)	E_a (kJ/mol)	$k_{25\,℃}$ ($mol/cm^2/s$)	E_a (kJ/mol)	m[a] (H^+)			
Quartz[b]	SiO_2	/	/	/	4.520×10^{-18}	90.1	3.240×10^{-22}	82.7	-0.500	890[c]	$(1–C)\times8.9$[h]	-
K-feldspar[b]	$KAlSi_3O_8$	8.710×10^{-15}	51.7	0.500	3.890×10^{-17}	38.0	6.310×10^{-26}	94.1	-0.823	1460[c]	*SF*×*SSA*[i]	-
Kaolinite[b]	$Al_2Si_2O_5(OH)_4$	4.897×10^{-16}	65.9	0.777	6.607×10^{-18}	22.2	8.913×10^{-22}	17.9	-0.472	132000[c]	*SF*×*SSA*[j]	100
Illite[b]	Muscovite ($KAl_3Si_3O_{10}(OH)_2$)	1.413×10^{-16}	22.0	0.370	2.818×10^{-18}	22.0	2.818×10^{-19}	22.0	-0.220	23600[d]	*SF*×*SSA*[j]	-
Chlorite[b]	$Clinochlore_{0.5}Daphnite_{0.5}$ ($Mg_{2.5}Fe_{2.5}Al_2Si_3O_{10}(OH)_8$)	7.762×10^{-16}	88.0	0.500	3.020×10^{-17}	88.0	/	/	/	76000[c]	*SF*×*SSA*[j]	-
Smectite[b]	Saponite-Ca ($Ca_{0.165}Mg_3Al_{0.33}Si_{3.67}O_{10}(OH)_2$)	1.047×10^{-15}	23.6	0.340	1.660×10^{-17}	35.0	3.020×10^{-21}	58.9	-0.400	1363000[c]	*SF*×*SSA*[j]	-
Siderite[b]	$FeCO_3$	5.900×10^{-10}	56.0	0.600	2.100×10^{-13}	56.0	/	/	/	1750[e]	0.0175[k]	10
Magnesite[b]	$MgCO_3$	4.169×10^{-11}	14.4	1.000	4.571×10^{-14}	23.5	/	/	/	662[f]	0.00662	10
Dolomite[b]	$CaMg(CO_3)_2$	6.457×10^{-8}	36.1	0.500	2.951×10^{-12}	52.2	/	/	/	1020[g]	0.0102	10

[a]$k_{25\,℃}$ = standard rate constant; E_a = activation energy; n and m = reaction orders with respect to H^+; *SSA* = specific surface area; *ESA* = effective surface area; *SF* = scaling factor.
[b]Rate parameters derived from Palandri and Kharaka (2004).
[c]Beckingham et al. (2016).
[d]Lammers et al. (2017).
[e]Golubev et al. (2009).
[f]Pokrovsky et al. (2009).
[g]Luhmann et al. (2014).
[h]*C* is the coating factor which is equivalent to the coat coverage. The *SF* for quartz is 0.01.
[i]The *SF* for K-feldspar is 0.01 for sub-arkose and arkose, while it is 0.00001 for quartz arenite.
[j]The *SF* for grain-coating clay minerals is 0.01 when gran-coating clay volumes are greater than 5 vol.%, while is 0.00001 when clay volumes are smaller than 5 vol.% (Beckingham et al., 2017).
[k]The *SF* for all secondary minerals is 0.00001.

Table S2. Diffusion coefficients of available species in free solutions at different temperatures.

Species		Diffusion coefficients in free solutions						T_c[b]	T_f[b]
		25 °C[a]	60 °C[a]	70 °C[a]	80 °C[a]	90 °C[a]	100 °C[a]		
Cations	H^+	8.69×10^{-5}	1.48×10^{-4}	1.63×10^{-4}	1.79×10^{-4}	1.94×10^{-4}	2.10×10^{-4}	54.40	1.555
	Na^+	1.26×10^{-5}	2.39×10^{-5}	2.69×10^{-5}	2.98×10^{-5}	3.28×10^{-5}	3.58×10^{-5}	6.06	0.297
	K^+	1.84×10^{-5}	3.41×10^{-5}	3.82×10^{-5}	4.23×10^{-5}	4.64×10^{-5}	5.05×10^{-5}	9.55	0.409
	Ca^{2+}	7.53×10^{-6}	1.43×10^{-5}	1.61×10^{-5}	1.79×10^{-5}	1.97×10^{-5}	2.15×10^{-5}	3.60	0.179
	Fe^{2+}	6.58×10^{-6}	1.23×10^{-5}	1.38×10^{-5}	1.53×10^{-5}	1.68×10^{-5}	1.83×10^{-5}	3.31	0.150
	Mg^{2+}	6.55×10^{-6}	1.21×10^{-5}	1.35×10^{-5}	1.50×10^{-5}	1.64×10^{-5}	1.78×10^{-5}	3.43	0.144
	Al^{3+}	6.61×10^{-6}	1.50×10^{-5}	1.70×10^{-5}	1.90×10^{-5}	2.10×10^{-5}	2.30×10^{-5}	3.00	0.200
	$Al(OH)_4^-$	9.82×10^{-6}	1.60×10^{-5}	1.80×10^{-5}	2.00×10^{-5}	2.20×10^{-5}	2.40×10^{-5}	4.00	0.200
Anions	OH^-	4.96×10^{-5}	9.15×10^{-5}	1.03×10^{-4}	1.13×10^{-4}	1.24×10^{-4}	1.35×10^{-4}	25.90	1.094
	HCO_3^-	1.11×10^{-5}	2.16×10^{-5}	2.43×10^{-5}	2.71×10^{-5}	2.98×10^{-5}	3.26×10^{-5}	5.06	0.275
	CO_3^{2-}	8.67×10^{-6}	1.63×10^{-5}	1.83×10^{-5}	2.03×10^{-5}	2.22×10^{-5}	2.42×10^{-5}	4.33	0.199
	Cl^-	1.92×10^{-5}	3.30×10^{-5}	3.70×10^{-5}	4.10×10^{-5}	4.50×10^{-5}	4.90×10^{-5}	9.00	0.400
Molecules	$SiO_{2(aq)}$	1.75×10^{-5}	3.50×10^{-5}	4.00×10^{-5}	4.50×10^{-5}	5.00×10^{-5}	5.50×10^{-5}	5.00	0.500
	CO_2	1.79×10^{-5}	2.50×10^{-5}	2.83×10^{-5}	3.15×10^{-5}	3.48×10^{-5}	3.80×10^{-5}	5.50	0.325
Average		/	3.56×10^{-5}	3.98×10^{-5}	4.40×10^{-5}	4.83×10^{-5}	5.25×10^{-5}	/	/

[a]Data at 25 °C was directly derived from the compilation by Schulz and Zabel (2006). Data at other temperatures was calculated in this work.

[b]T_c and T_f for Al^{3+}, $Al(OH)_4^-$, and Cl^- were derived by fitting the data to the Eq. 19 (Park, 2014), which was conducted in this work. T_c and T_f for other species were directly derived from Park (2014).

2. Water-CO_2-rock interactions in smectite coats using variable grain sizes

As a result of grain size rising from 0.04 (siltstone) to 1 mm (coarse sandstone), pH gradually increases (Fig. S1(A)) and HCO_3^-, $CO_{2(aq)}$, and $CO_{2(g)}$ gradually decrease (Fig. S1(B)-S1(D)). Regarding the dissolution of primary minerals, the precipitation of secondary minerals, increasing grain size results in significantly lower smectite dissolution (Fig. S1(E)), slightly higher K-feldspar dissolution (Fig. S1(F)), significantly lower kaolinite precipitation (Fig. S1(G)), slightly lower precipitation of magnesite and dolomite (Fig. S1(I)-S1(J)), slightly lower mineral carbonation (Fig. S1(K)), and slightly lower net porosity increase (Fig. S1(L)).

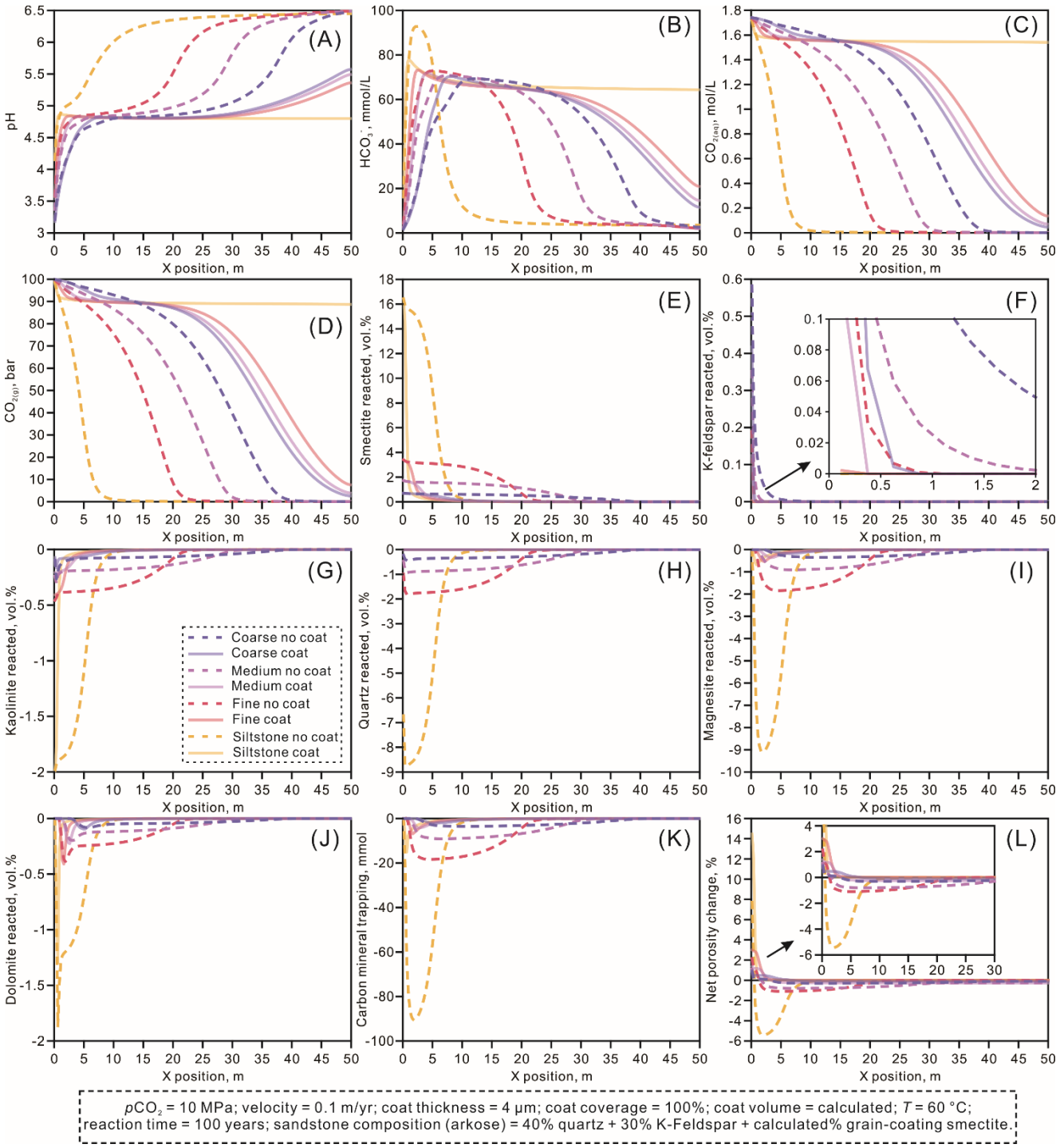

Fig. S1. Changes in water pH (A), CO_2 speciation (B–D), mineral dissolution and precipitation (E–J), mineral trapping of CO_2 (K), and net porosity changes (L) using different detrital grain sizes after the injection of CO_2 over 100 years.

For four grain sizes, pore-filling scenario consistently results in significantly higher pH (Fig. S1A), lower HCO_3^-, $CO_{2(aq)}$, and $CO_{2(g)}$ (Fig. S1(B)-S1(D)), significantly higher dissolution of smectite and K-feldspar (Fig. S1(E)-S1(F)), significantly higher precipitation of kaolinite, quartz, magnesite, and dolomite (Fig. S1(E)-S1(J)), significantly higher mineral carbonation (Fig. S1(K)). Moreover, grain-

coating scenarios only result in net porosity increase, while net porosity decreases were also observed for pore-filling scenarios (Fig. S1L).

3. Water-CO_2-rock interactions in smectite coats using variable detrital lithologies

For the three utilized detrital sandstone lithologies (quartz arenite, sub-arkose and arkose sandstones), Fig. S2 illustrates that there are no identifiable changes in every examined parameter, indicating that detrital lithology has no influences on water-CO_2-rock interactions in smectite-coated sandstones. Furthermore, there are also no differences or only minor differences in the examined parameters among different detrital lithologies for the pore-filling scenarios (Fig. S2).

However, pore-filling scenarios result in significant differences in the examined parameters compared to the grain-coating scenarios (Fig. S2), which is consistent with the difference between pore-filling scenario and grain-coating scenario of 100% coat coverage as described in Section 3.2.1. In general, pore-filling scenario results in significantly higher pH, lower HCO_3^-, $CO_{2(aq)}$, and $CO_{2(g)}$, higher dissolution of smectite and K-feldspar, higher precipitation of quartz, kaolinite, magnesite and dolomite, higher mineral carbonation, and higher net porosity decrease (Fig. S2).

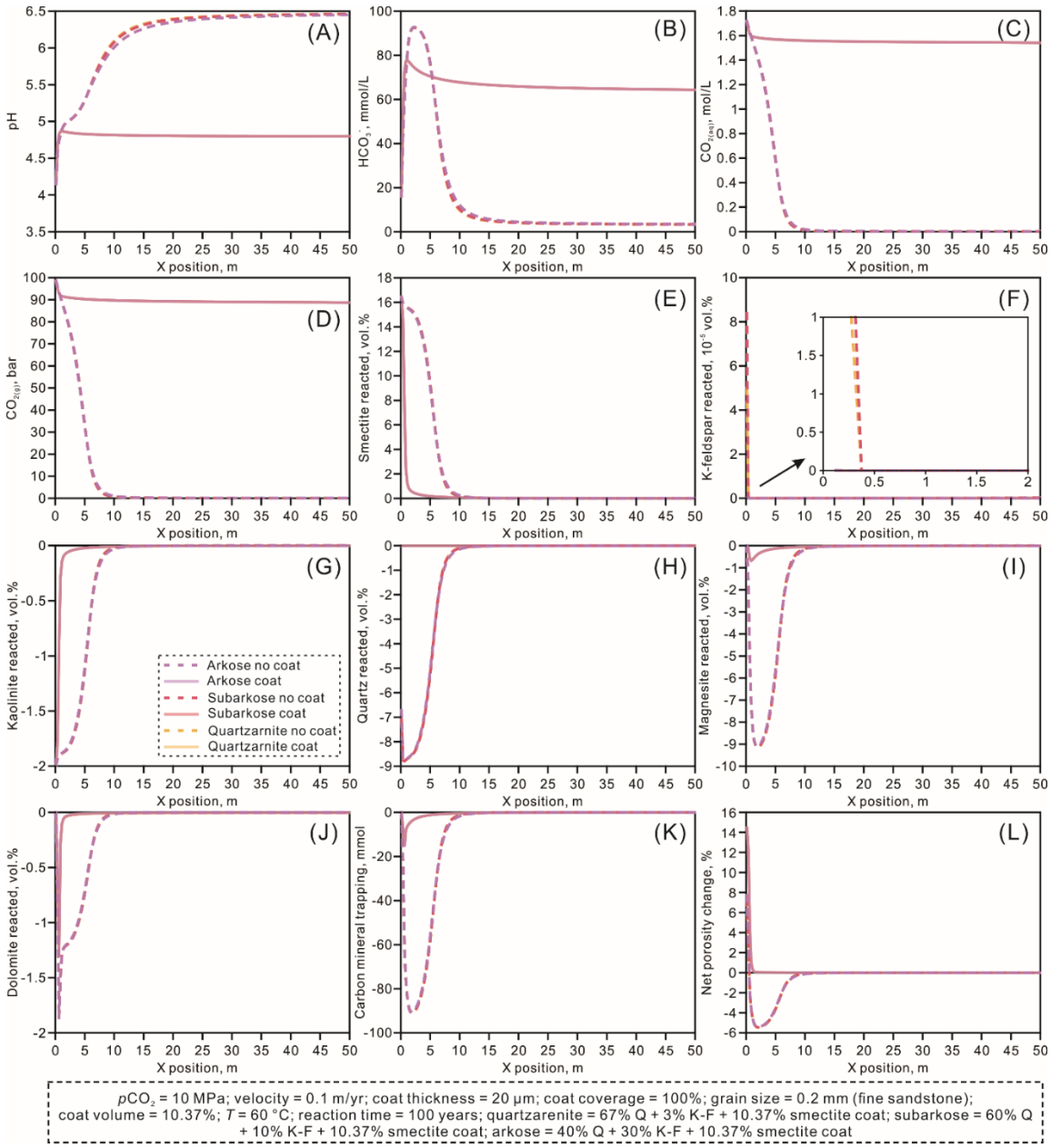

Fig. S2. Changes in water pH (A), CO_2 speciation (B–D), mineral dissolution and precipitation (E–J), mineral trapping of CO_2 (K), and net porosity changes (L) using different detrital lithologies after the injection of CO_2 over 100 years.

4. Water-CO_2-rock interactions in smectite coats considering the deceleration of K-feldspar dissolution rate

4.1. Method achieving the decelerating effect of clay coats on the dissolution of K-feldspar

To our knowledge, a well-established theory accounting for the decelerating effect of clay coats on the dissolution of minerals being covered is reported by Emmanuel (2022). In this study, the author

constructed a numerical model in which primary minerals were coated with a continuous (100% coverage) insoluble mineral layer. The insoluble coating layer is porous and therefore allows solutes to diffuse through the layer. Emmanuel (2022) considered three main factors that may constrain the effect of coating phase on primary mineral dissolution, including the thickness of coating phase, the ratio (ε) of microporosity (ø) the coating phase over tortuosity (θ) of the coating phase, and the ratio of the dissolution rate of the mineral being covered to the mass diffusion rate in the coating mineral (defined as Biot number). The Biot number for the weathering of silicate minerals are very low (Emmanuel, 2022). Therefore, the layer thickness and ε were likely to play predominant roles. The ε is estimated as (Boudreau, 1997; Li et al., 2025):

$$\varepsilon = \frac{ø}{\theta} = \frac{ø}{1-\ln(ø^2)}. \quad \text{(S1)}$$

Based on the microporosities of grain-coating clays (see Section 2.4), the calculated ε values for chlorite, smectite, illite, and kaolinite are 0.324, 0.069, 0.199, and 0.279, respectively. If a maximum thickness of the coating mineral is 20 μm, the dissolution rate of the mineral being covered would be maximumly decreased by three orders of magnitude (Emmanuel, 2022). To discuss the influence of such an effect, we artificially decreased K-feldspar dissolution rate with 1, 2 and 3 orders of magnitudes. In comparison, as quartz does not dissolve in all models (see Section 3.1), the decelerating effect of clay coats on quartz dissolution was not considered in all models.

4.2. Modelling results

The dissolution rate of detrital K-feldspar was artificially decreased by 10^{-1} to 10^{-3}. However, Fig. S3 illustrates that there are no identifiable differences in the examined parameters among different dissolution rate reductions of K-feldspar, indicating that the potential K-feldspar dissolution rate deceleration does not have identifiable influences on the examined geochemical parameters in the models for smectite coats. Furthermore, for pore-filling scenarios, it is also indicated that the K-feldspar dissolution rate deceleration does not have identifiable influences on water-CO_2-rock interactions (Fig. S3).

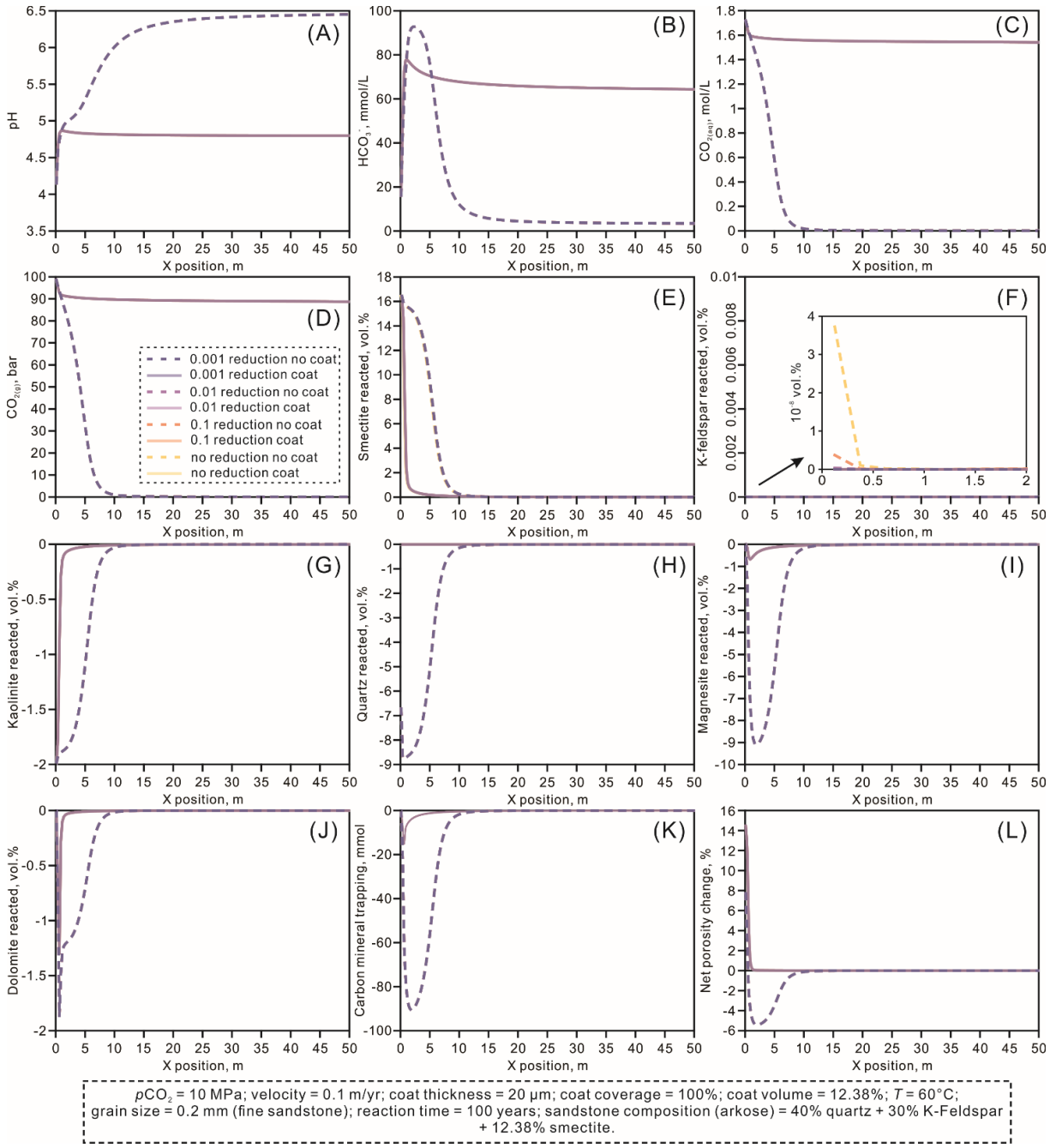

Fig. S3. Changes in water pH (A), CO_2 speciation (B–D), mineral dissolution and precipitation (E–J), mineral trapping of CO_2 (K), and net porosity changes (L) using different orders of reduction in K-feldspar dissolution rate after the injection of CO_2 over 100 years.

5. Water-CO_2-rock interactions in chlorite-coated sandstones

5.1. Water-CO_2-rock interactions using variable chlorite coat parameters

5.1.1. Variable coat coverages

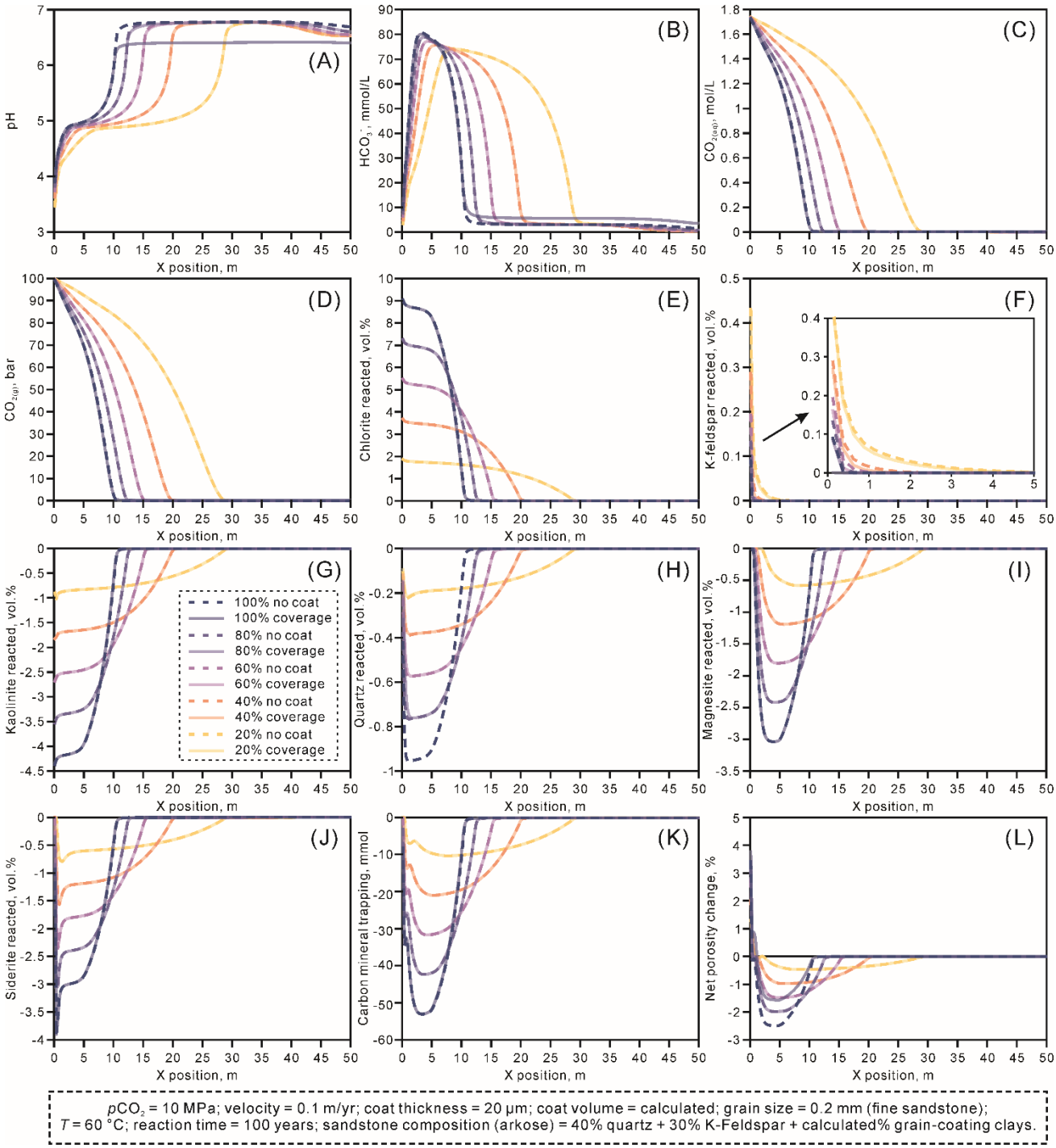

Fig. S4. Changes in water pH (A), CO_2 speciation (B–D), mineral dissolution and precipitation (E–J), mineral trapping of CO_2 (K), and net porosity changes (L) using different coat coverages after the injection of CO_2 over 100 years. In panels E–K, positive values indicate mineral dissolution, while negative values indicate mineral precipitation. In the panel L, positive

values indicate net porosity increase, while negative values indicate net porosity decrease. Carbon mineral trapping (K) was calculated by summating the millimoles of secondary carbonates normalized to one C atom. pCO_2 = partial pressure of injecting CO_2 gas.

5.1.2. Variable coat thicknesses

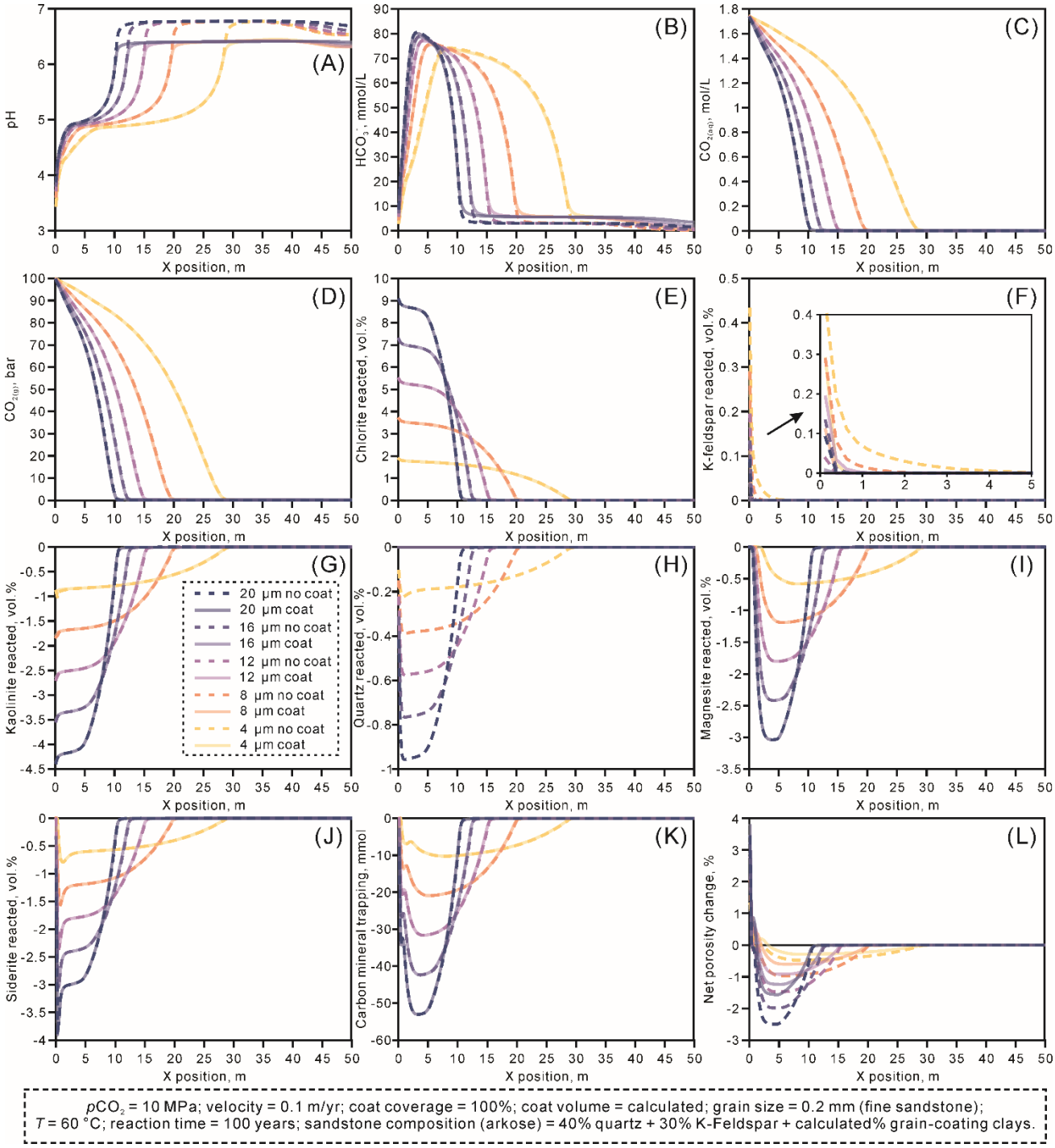

Fig. S5. Changes in water pH (A), CO_2 speciation (B–D), mineral dissolution and precipitation (E–J), mineral trapping of CO_2 (K), and net porosity changes (L) using different coat thicknesses after the injection of CO_2 over 100 years. In panels E–K, positive values indicate mineral dissolution, while negative values indicate mineral precipitation. In the panel L, positive values indicate net porosity increase, while negative values indicate net porosity decrease. Carbon mineral trapping

(K) was calculated by summating the millimoles of secondary carbonates normalized to one C atom. pCO_2 = partial pressure of injecting CO_2 gas.

5.2. Water-CO_2-rock interactions using variable grain sizes

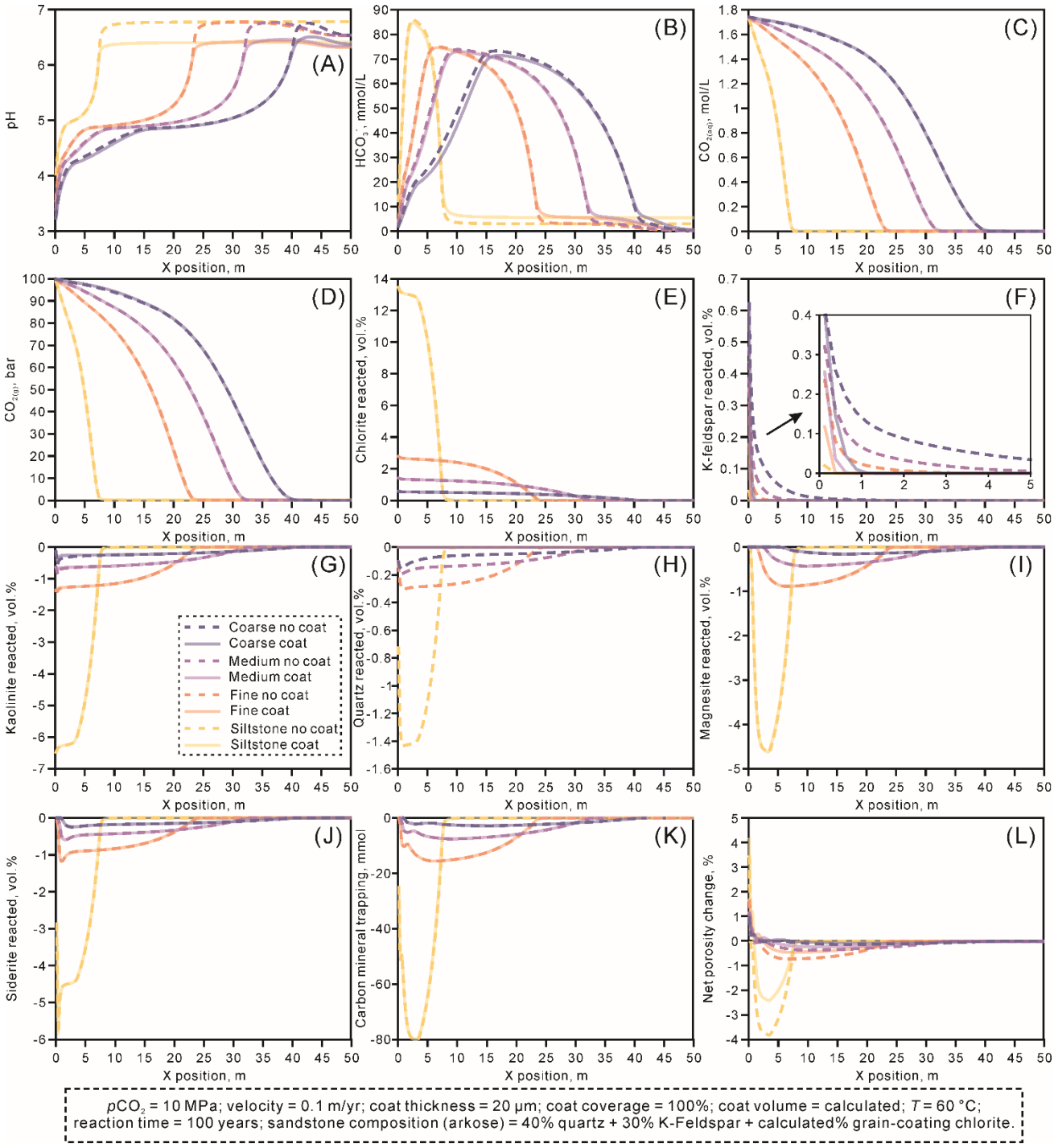

Fig. S6. Changes in water pH (A), CO_2 speciation (B–D), mineral dissolution and precipitation (E–J), mineral trapping of CO_2 (K), and net porosity changes (L) using different grain sizes after the injection of CO_2 over 100 years. In panels E–K, positive values indicate mineral dissolution, while negative values indicate mineral precipitation. In the panel L, positive values indicate net porosity increase, while negative values indicate net porosity decrease. Carbon mineral trapping (K) was

calculated by summating the millimoles of secondary carbonates normalized to one C atom. pCO_2 = partial pressure of injecting CO_2 gas.

5.3. Water-CO_2-rock interactions using variable detrital lithologies

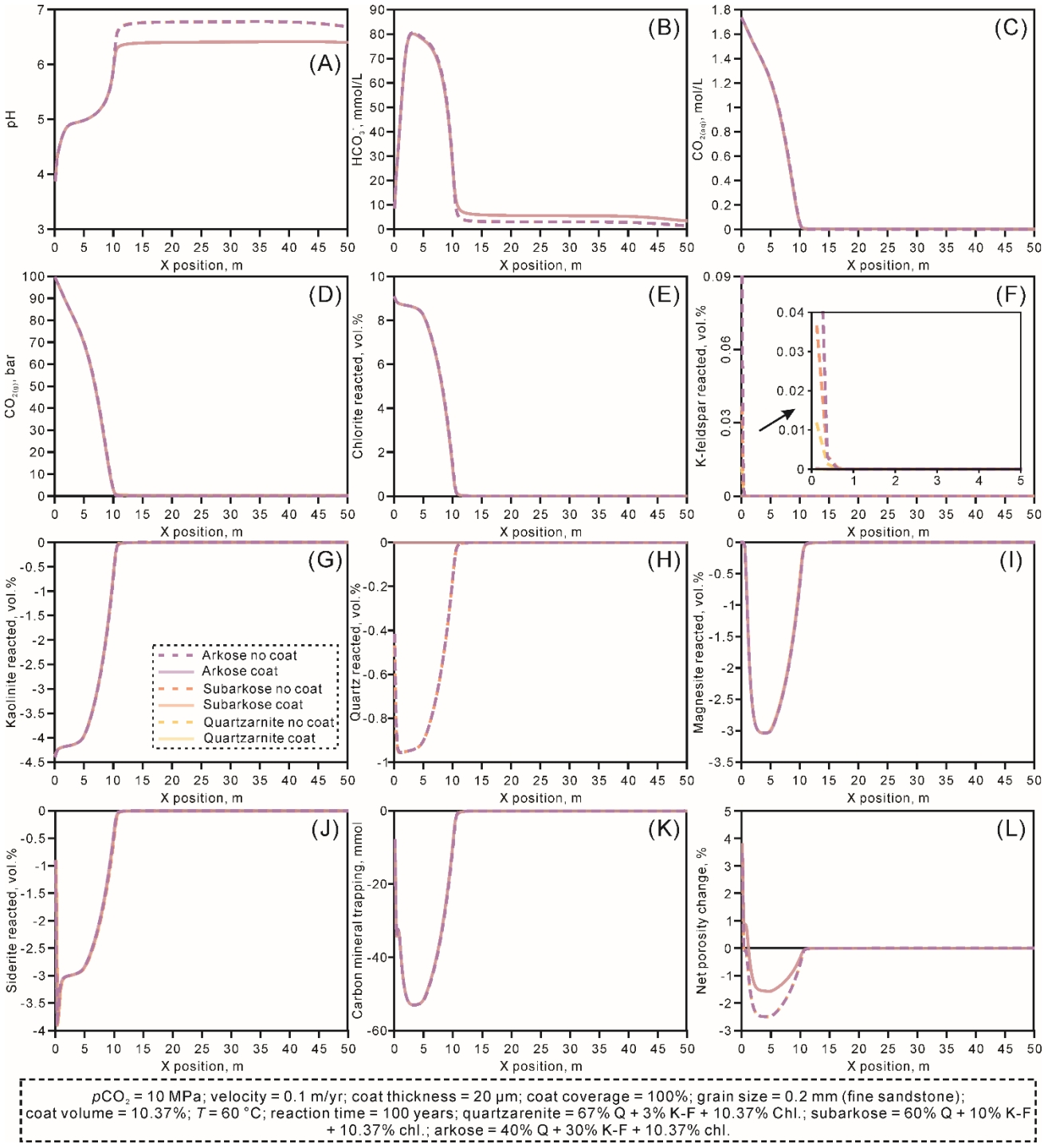

Fig. S7. Changes in water pH (A), CO_2 speciation (B–D), mineral dissolution and precipitation (E–J), mineral trapping of CO_2 (K), and net porosity changes (L) using different detrital lithologies after the injection of CO_2 over 100 years. In panels E–K, positive values indicate mineral dissolution, while negative values indicate mineral precipitation. In the panel L, positive values indicate net porosity increase, while negative values indicate net porosity decrease. Carbon mineral trapping

(K) was calculated by summating the millimoles of secondary carbonates normalized to one C atom. pCO_2 = partial pressure of injecting CO_2 gas.

5.4. Water-CO_2-rock interactions using variable pCO_2

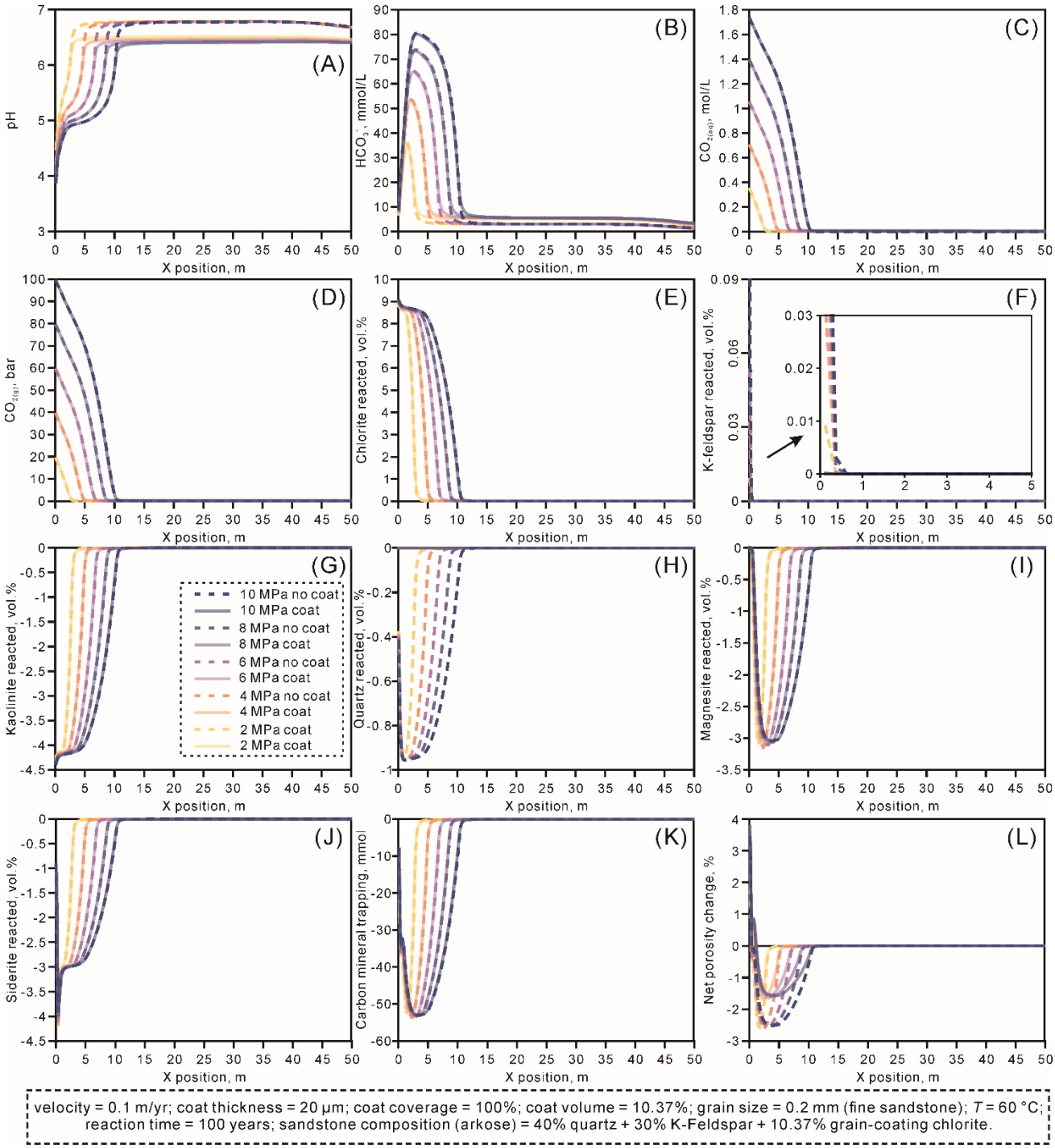

Fig. S8. Changes in water pH (A), CO_2 speciation (B–D), mineral dissolution and precipitation (E–J), mineral trapping of CO_2 (K), and net porosity changes (L) using different partial pressures of injecting CO_2 gas (pCO_2) over 100 years. In panels E–K, positive values indicate mineral dissolution, while negative values indicate mineral precipitation. In the panel L, positive values indicate net porosity increase, while negative values indicate net porosity decrease. Carbon mineral trapping (K) was calculated by summating the millimoles of secondary carbonates normalized to one C atom.

5.5. Water-CO_2-rock interactions using variable temperatures

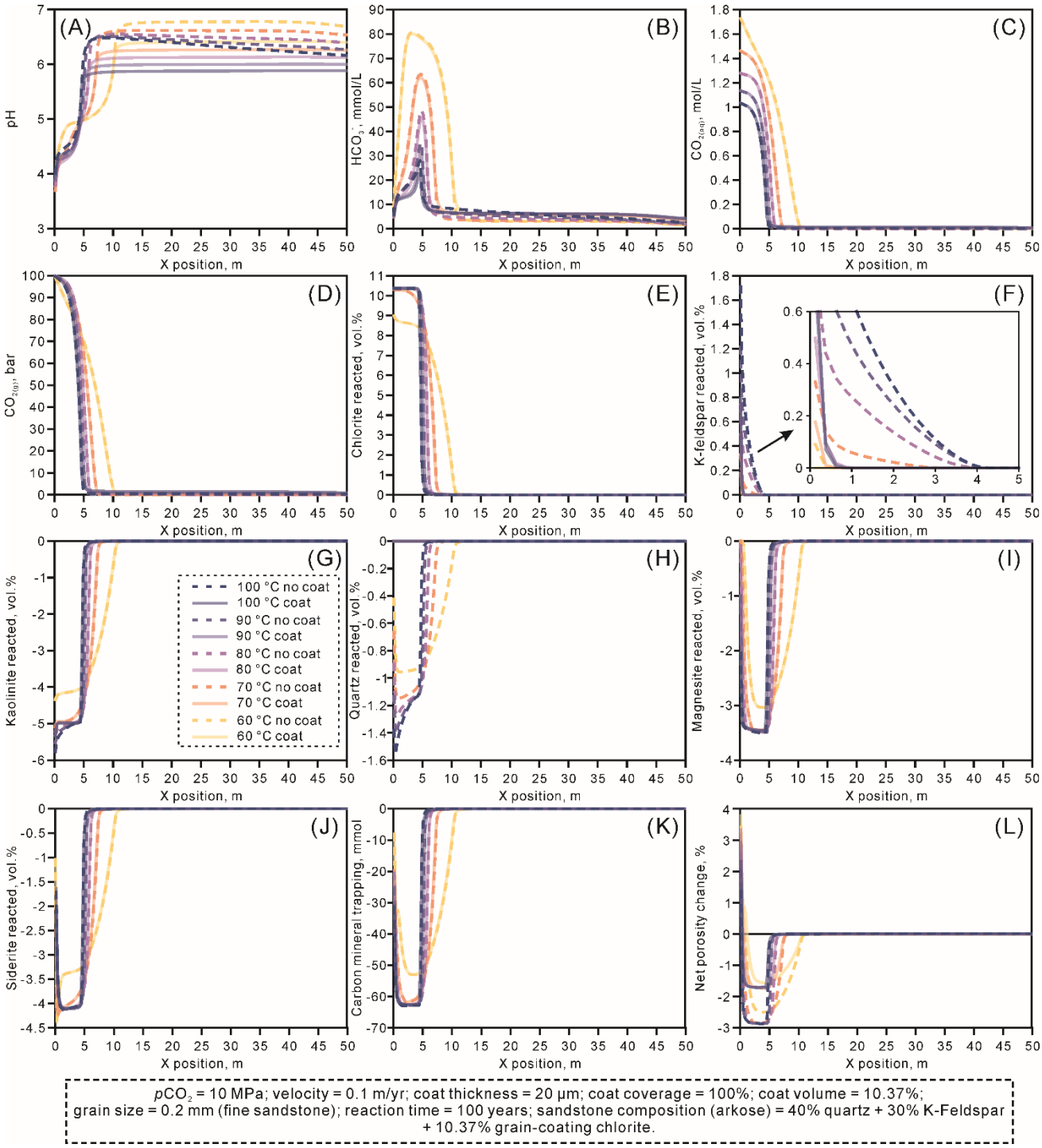

Fig. S9. Changes in water pH (A), CO_2 speciation (B–D), mineral dissolution and precipitation (E–J), mineral trapping of CO_2 (K), and net porosity changes (L) using different temperatures after the injection of CO_2 over 100 years. In panels E–K, positive values indicate mineral dissolution, while negative values indicate mineral precipitation. In the panel L, positive values indicate net porosity increase, while negative values indicate net porosity decrease. Carbon mineral trapping (K) was calculated by summating the millimoles of secondary carbonates normalized to one C atom.

5.6. Water-CO_2-rock interactions using variable fluid velocities

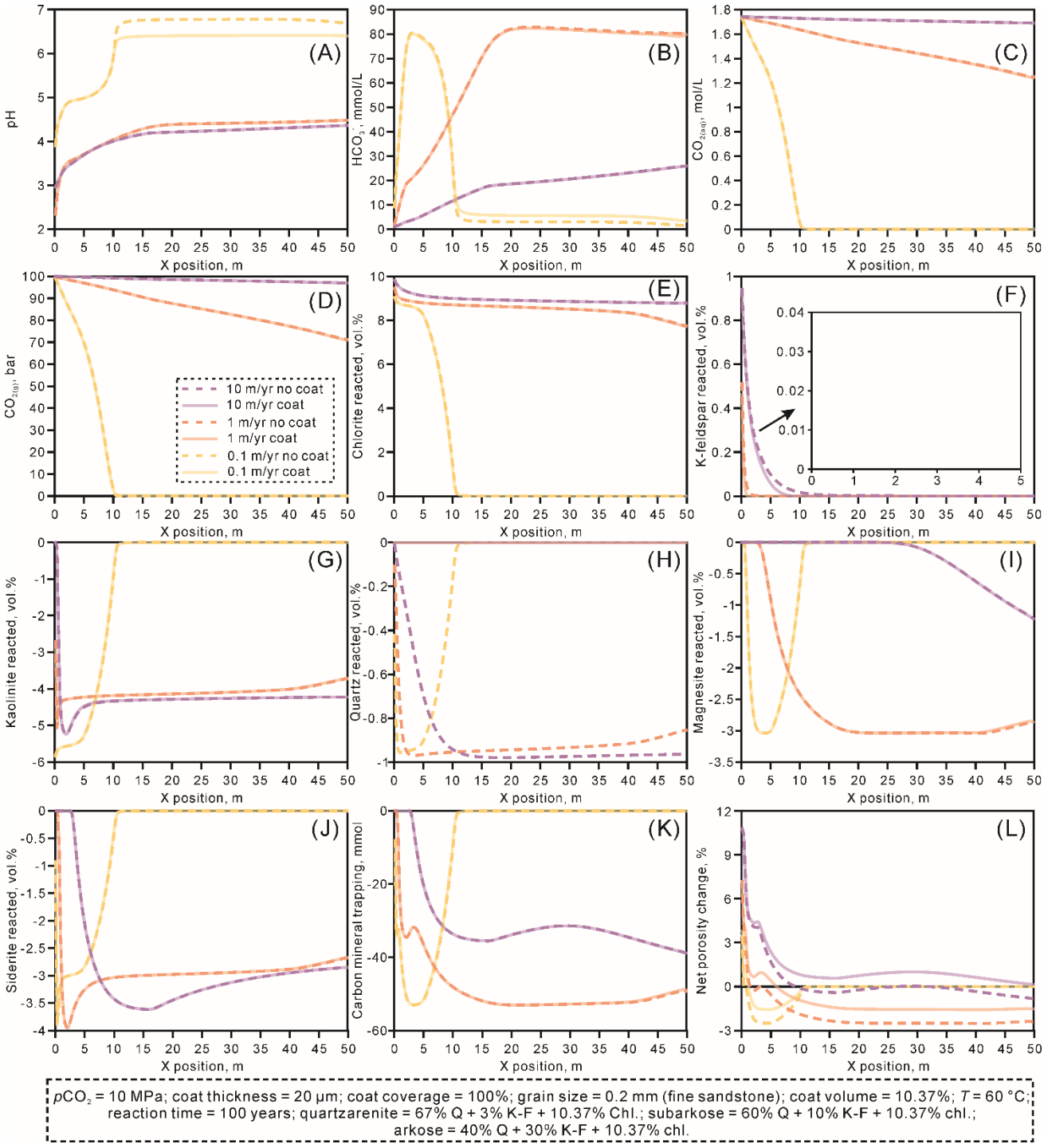

Fig. S10. Changes in water pH (A), CO_2 speciation (B–D), mineral dissolution and precipitation (E–J), mineral trapping of CO_2 (K), and net porosity changes (L) using different flow velocities after the injection of CO_2 over 100 years. In panels E–K, positive values indicate mineral dissolution, while negative values indicate mineral precipitation. In the panel L, positive values indicate net porosity increase, while negative values indicate net porosity decrease. Carbon mineral trapping (K) was calculated by summating the millimoles of secondary carbonates normalized to one C atom.

5.7. Water-CO_2-rock interactions with the incorporation of the reduction of dissolution rates of detrital grains

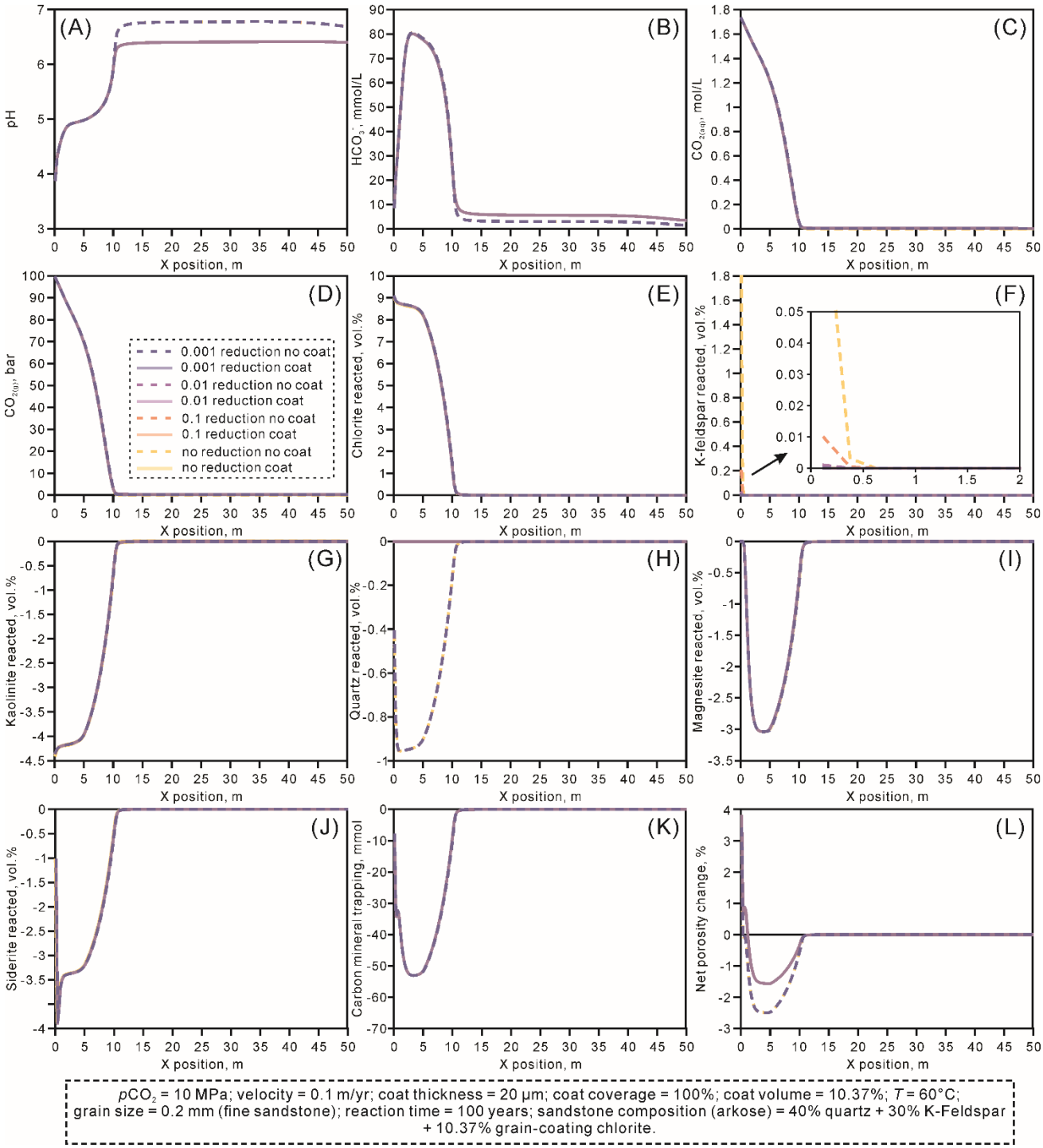

Fig. S11. Changes in water pH (A), CO_2 speciation (B–D), mineral dissolution and precipitation (E–J), mineral trapping of CO_2 (K), and net porosity changes (L) with the incorporation of the reduction of K-feldspar dissolution rate after the injection of CO_2 over 100 years. In panels E–K, positive values indicate mineral dissolution, while negative values indicate mineral precipitation. In the panel L, positive values indicate net porosity increase, while negative values indicate net porosity

decrease. Carbon mineral trapping (K) was calculated by summating the millimoles of secondary carbonates normalized to one C atom.

6. Water-CO_2-rock interactions in kaolinite-coated sandstones

6.1. Water-CO_2-rock interactions using variable kaolinite coat parameters

6.1.1. Variable coat coverages

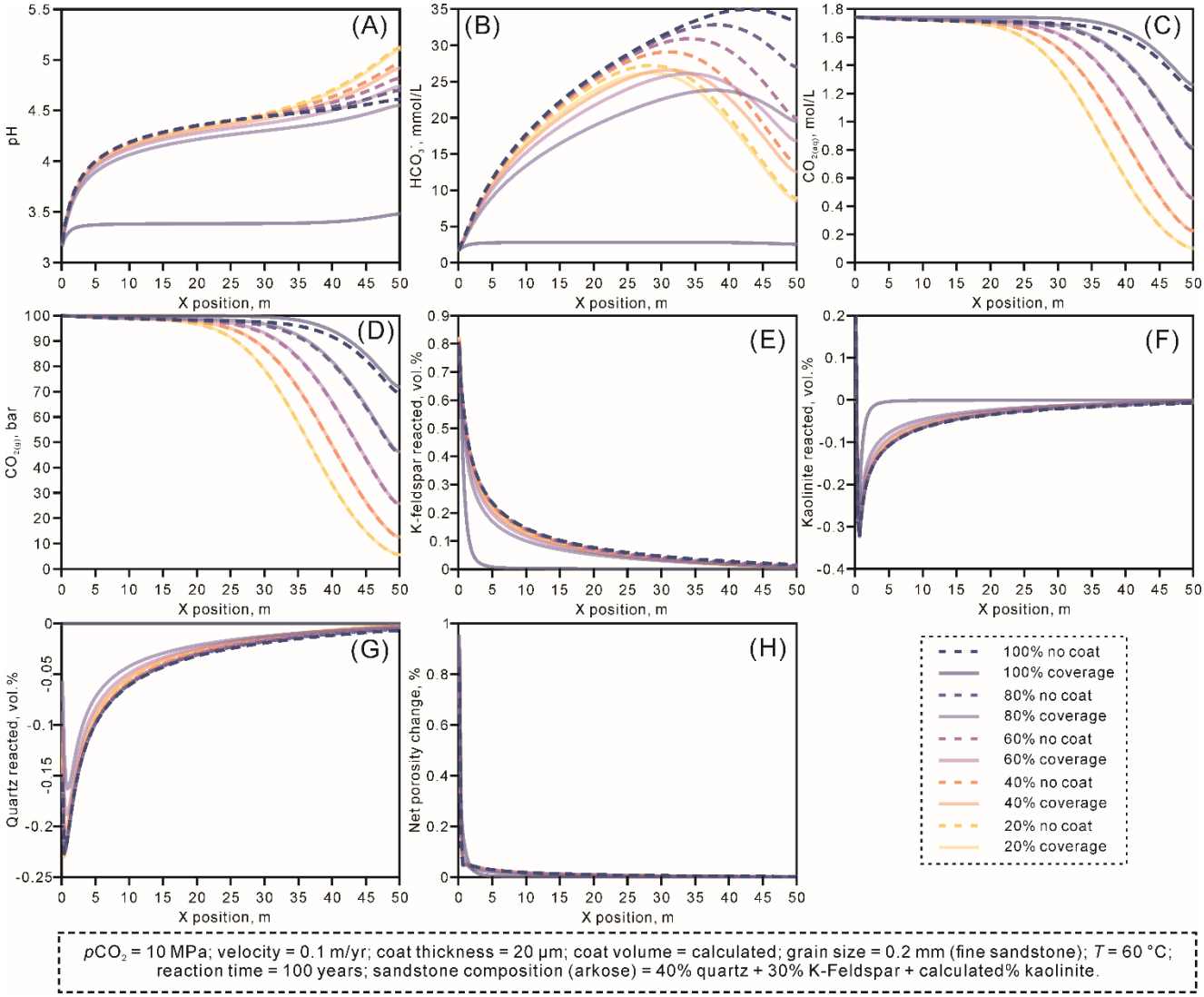

Fig. S12. Changes in water pH (A), CO_2 speciation (B–D), mineral dissolution and precipitation (E–G), and net porosity changes (H) using different coat coverages after the injection of CO_2 over 100 years. In panels E–G, positive values indicate mineral dissolution, while negative values indicate mineral precipitation. In the panel H, positive values indicate net porosity increase, while negative values indicate net porosity decrease. pCO_2 = partial pressure of injecting CO_2 gas.

6.1.2. Variable coat thicknesses

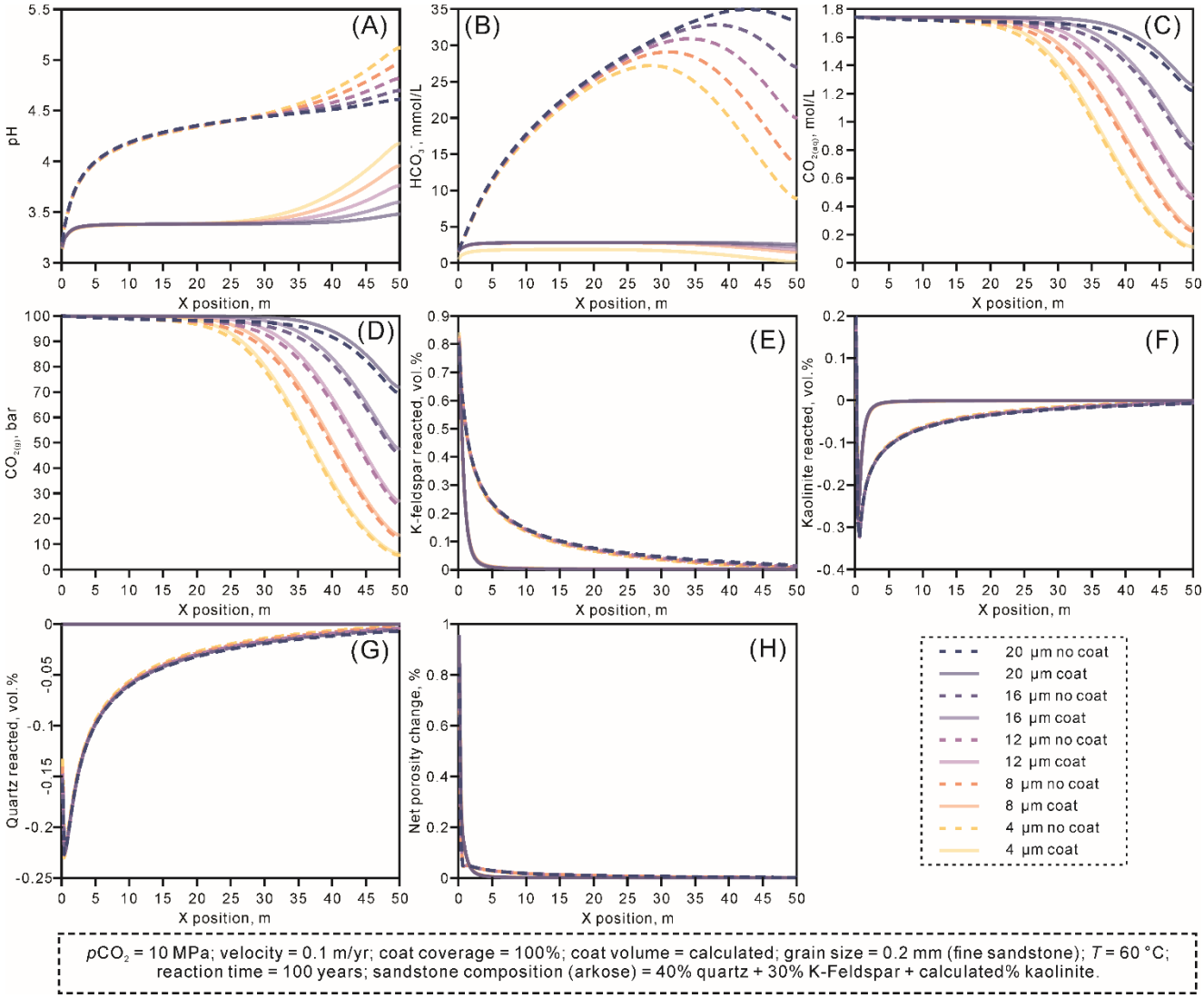

Fig. S13. Changes in water pH (A), CO_2 speciation (B–D), mineral dissolution and precipitation (E–G), and net porosity changes (H) using different coat thicknesses after the injection of CO_2 over 100 years. In panels E–G, positive values indicate mineral dissolution, while negative values indicate mineral precipitation. In the panel H, positive values indicate net porosity increase, while negative values indicate net porosity decrease. pCO_2 = partial pressure of injecting CO_2 gas.

6.2. Water-CO_2-rock interactions using variable grain sizes

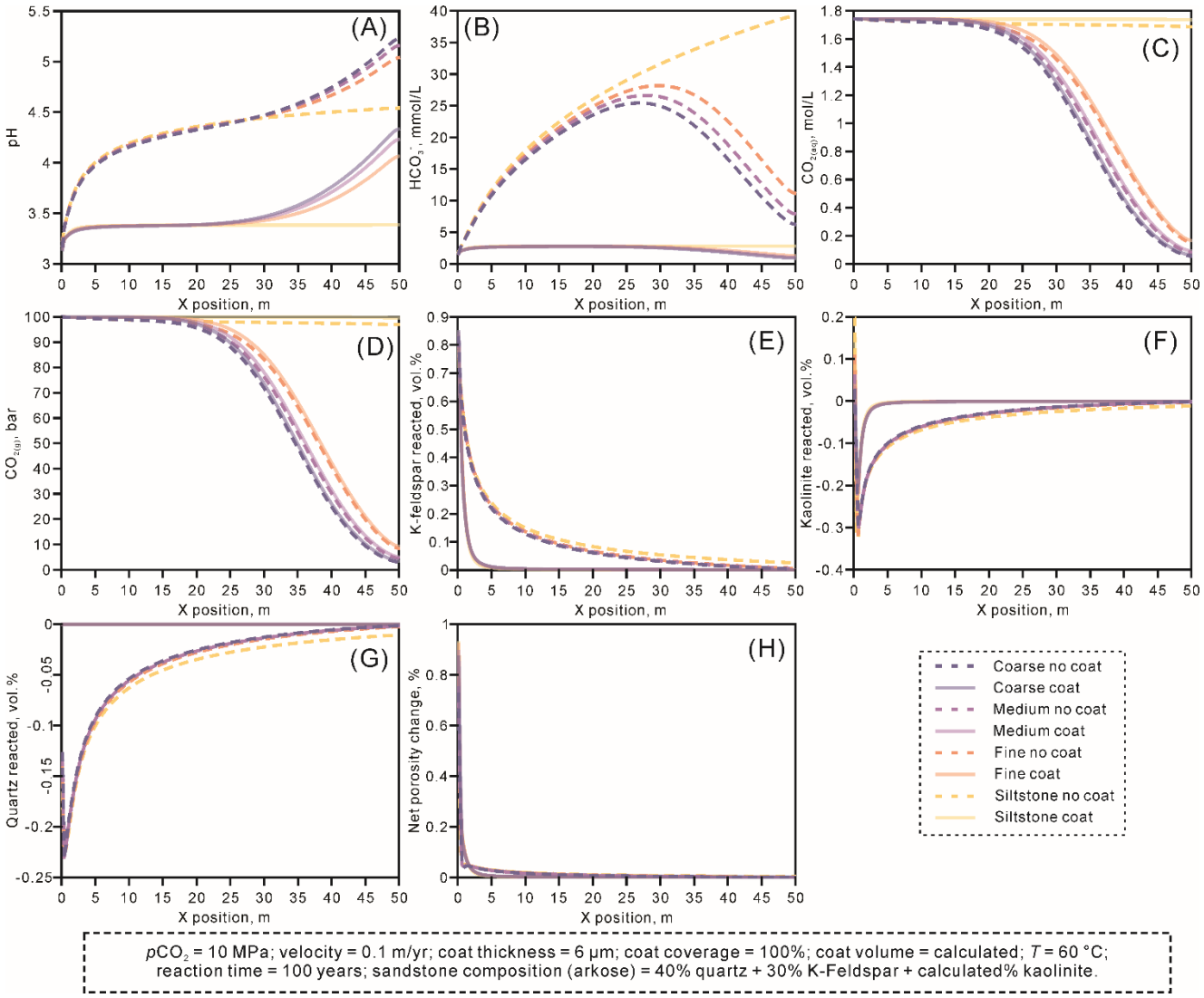

Fig. S14. Changes in water pH (A), CO_2 speciation (B–D), mineral dissolution and precipitation (E–G), and net porosity changes (H) using different grain sizes after the injection of CO_2 over 100 years. In panels E–G, positive values indicate mineral dissolution, while negative values indicate mineral precipitation. In the panel H, positive values indicate net porosity increase, while negative values indicate net porosity decrease. pCO_2 = partial pressure of injecting CO_2 gas.

6.3. Water-CO_2-rock interactions using variable detrital lithologies

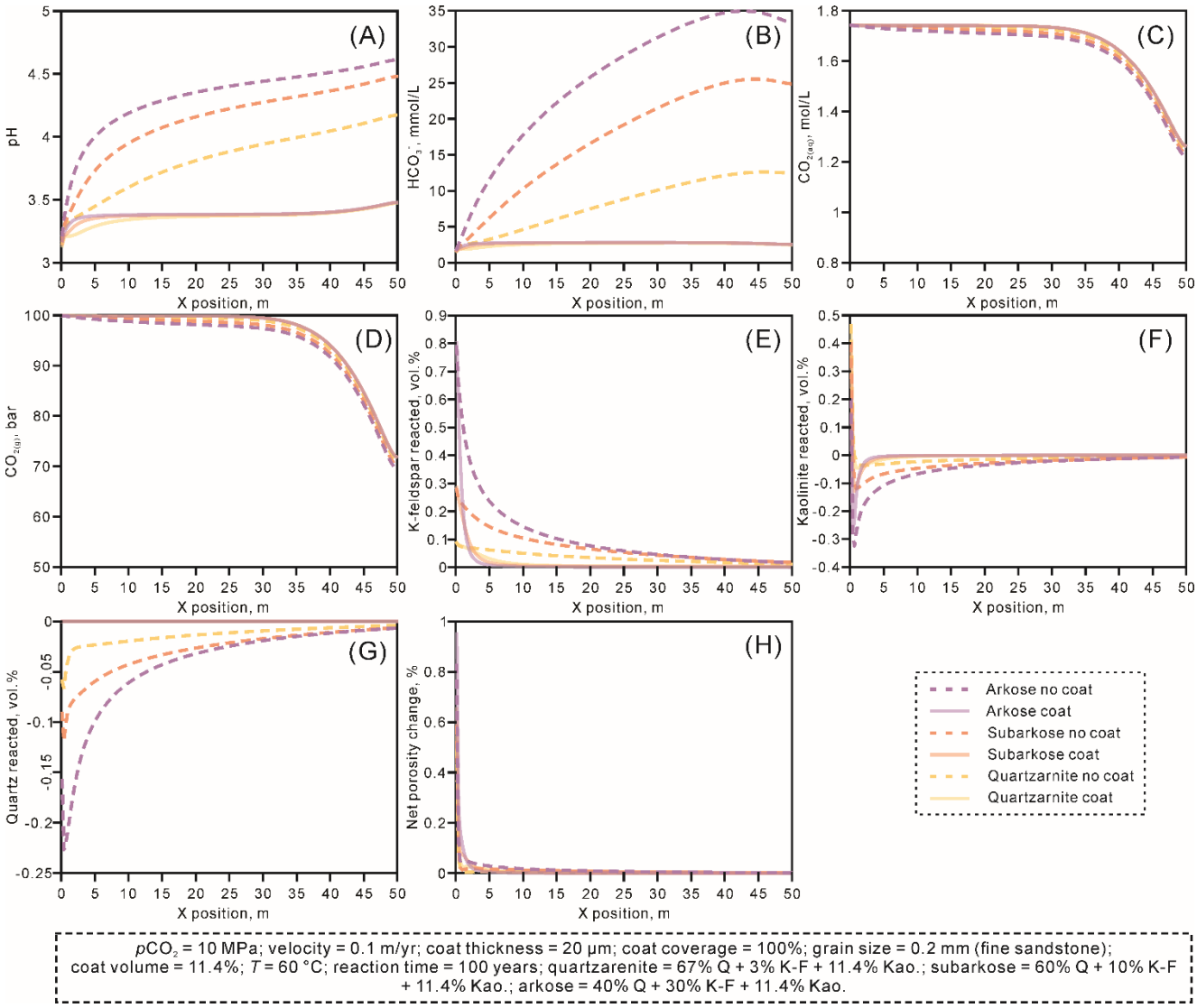

Fig. S15. Changes in water pH (A), CO_2 speciation (B–D), mineral dissolution and precipitation (E–G), and net porosity changes (H) using different detrital lithologies after the injection of CO_2 over 100 years. In panels E–G, positive values indicate mineral dissolution, while negative values indicate mineral precipitation. In the panel H, positive values indicate net porosity increase, while negative values indicate net porosity decrease. pCO_2 = partial pressure of injecting CO_2 gas.

6.4. Water-CO_2-rock interactions using variable pCO_2

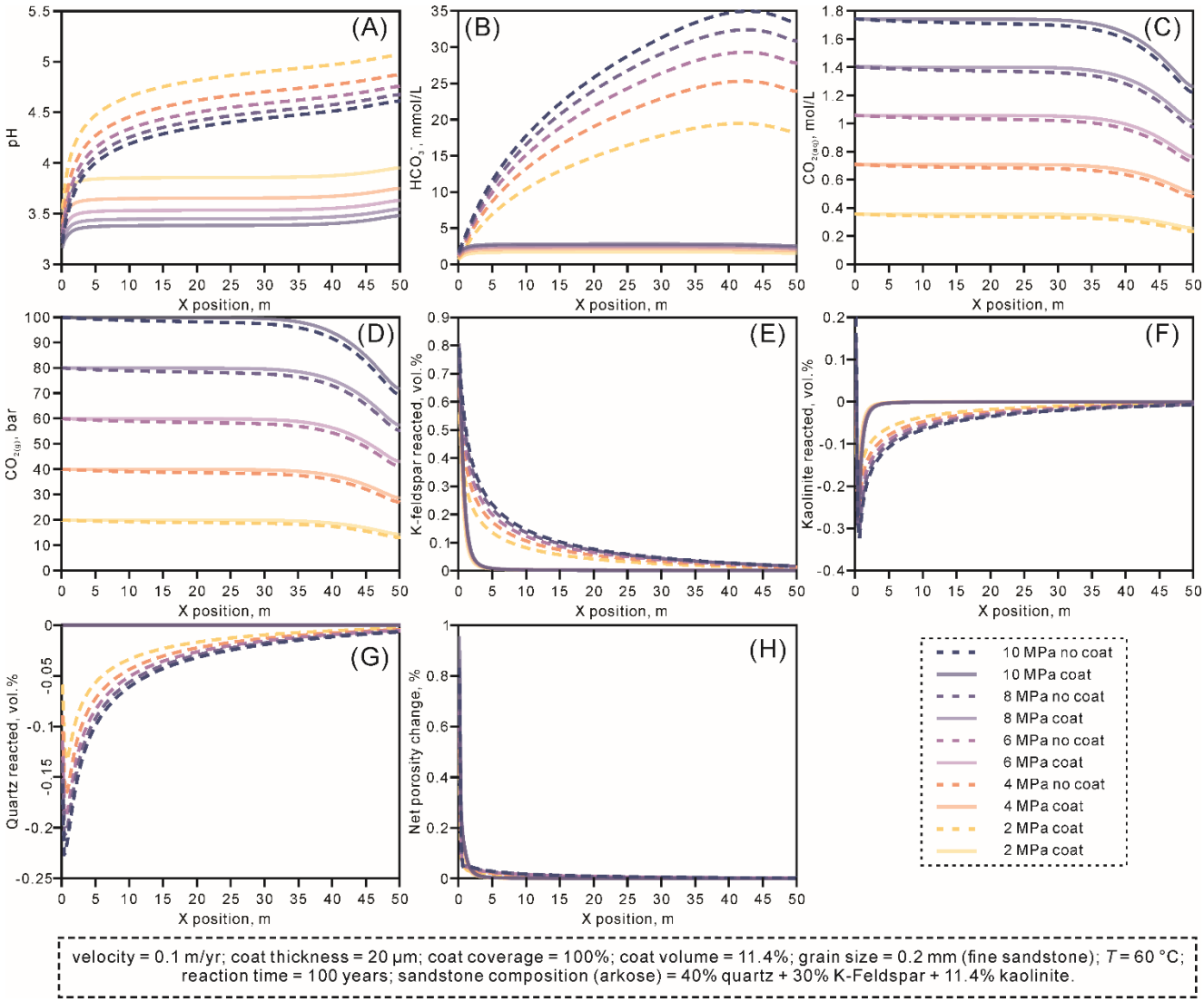

Fig. S16. Changes in water pH (A), CO_2 speciation (B–D), mineral dissolution and precipitation (E–G), and net porosity changes (H) using different partial pressures of injecting CO_2 gas (pCO_2) after the injection of CO_2 over 100 years. In panels E–G, positive values indicate mineral dissolution, while negative values indicate mineral precipitation. In the panel H, positive values indicate net porosity increase, while negative values indicate net porosity decrease.

6.5. Water-CO_2-rock interactions using variable temperatures

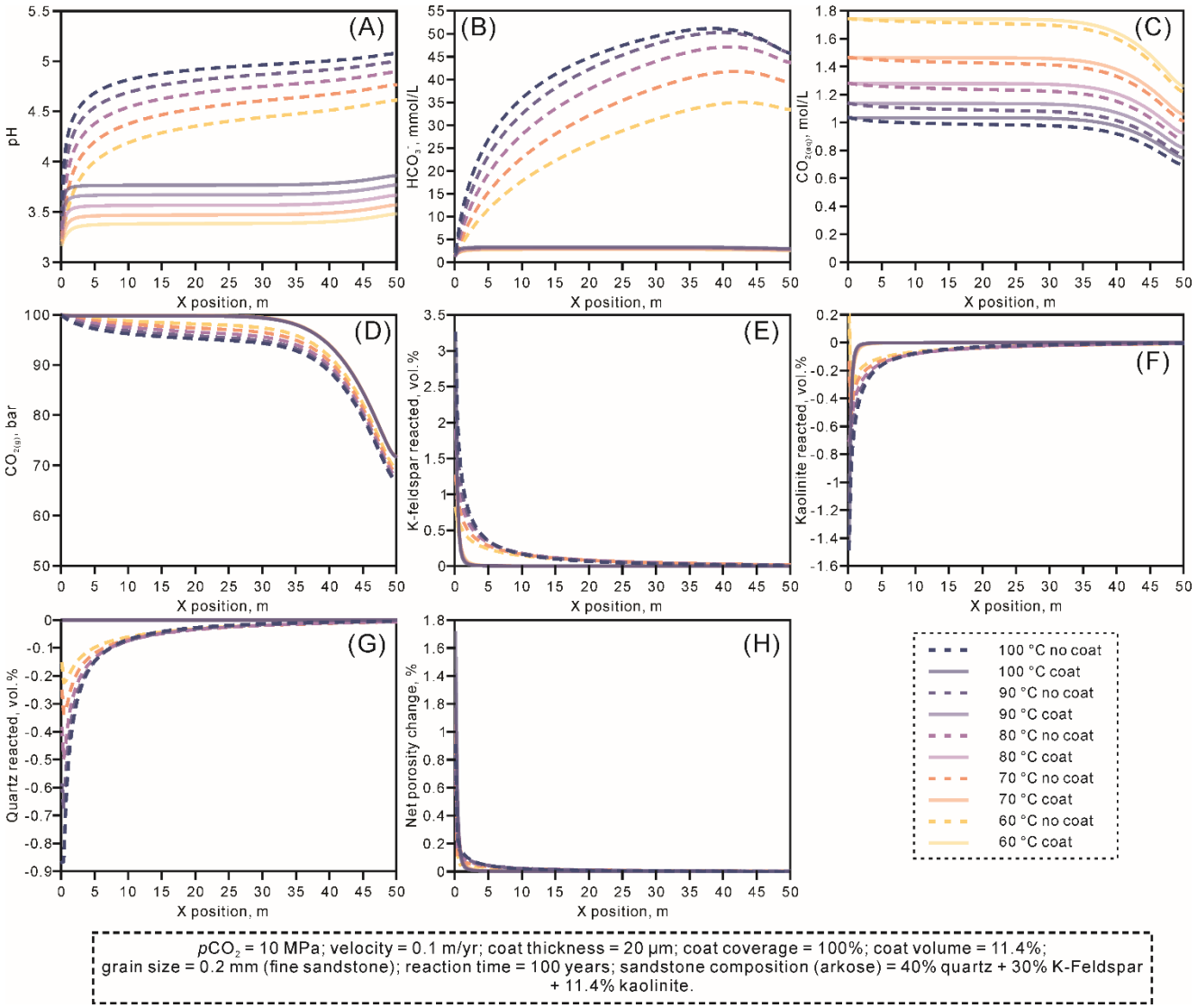

Fig. S17. Changes in water pH (A), CO_2 speciation (B–D), mineral dissolution and precipitation (E–G), and net porosity changes (H) using different temperatures after the injection of CO_2 over 100 years. In panels E–G, positive values indicate mineral dissolution, while negative values indicate mineral precipitation. In the panel H, positive values indicate net porosity increase, while negative values indicate net porosity decrease. pCO_2 = partial pressure of injecting CO_2 gas.

6.6. Water-CO_2-rock interactions using variable fluid velocities

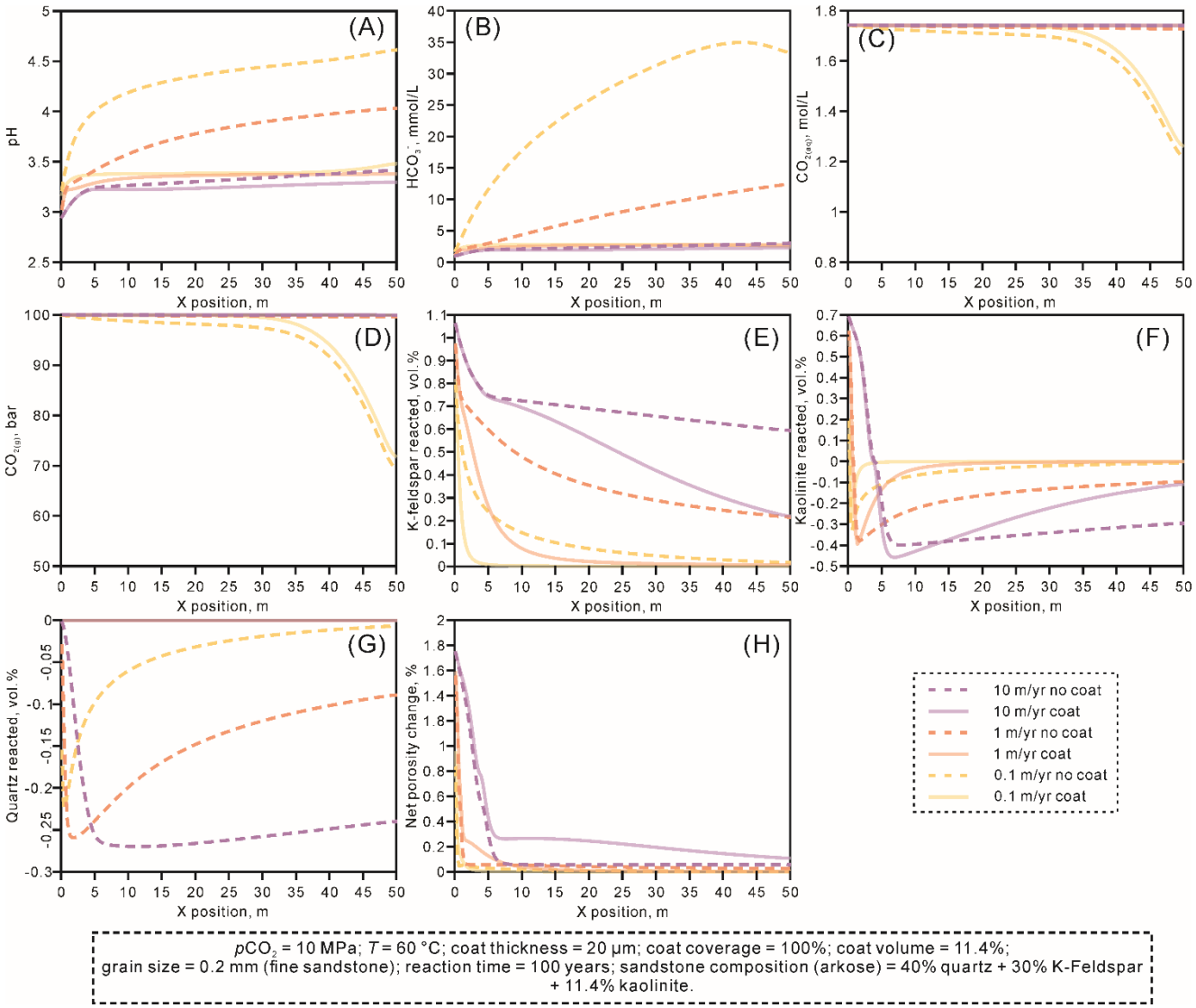

Fig. S18. Changes in water pH (A), CO_2 speciation (B–D), mineral dissolution and precipitation (E–G), and net porosity changes (H) using different fluid velocities after the injection of CO_2 over 100 years. In panels E–G, positive values indicate mineral dissolution, while negative values indicate mineral precipitation. In the panel H, positive values indicate net porosity increase, while negative values indicate net porosity decrease. pCO_2 = partial pressure of injecting CO_2 gas.

6.7. Water-CO_2-rock interactions with the incorporation of the reduction of dissolution rates of detrital grains

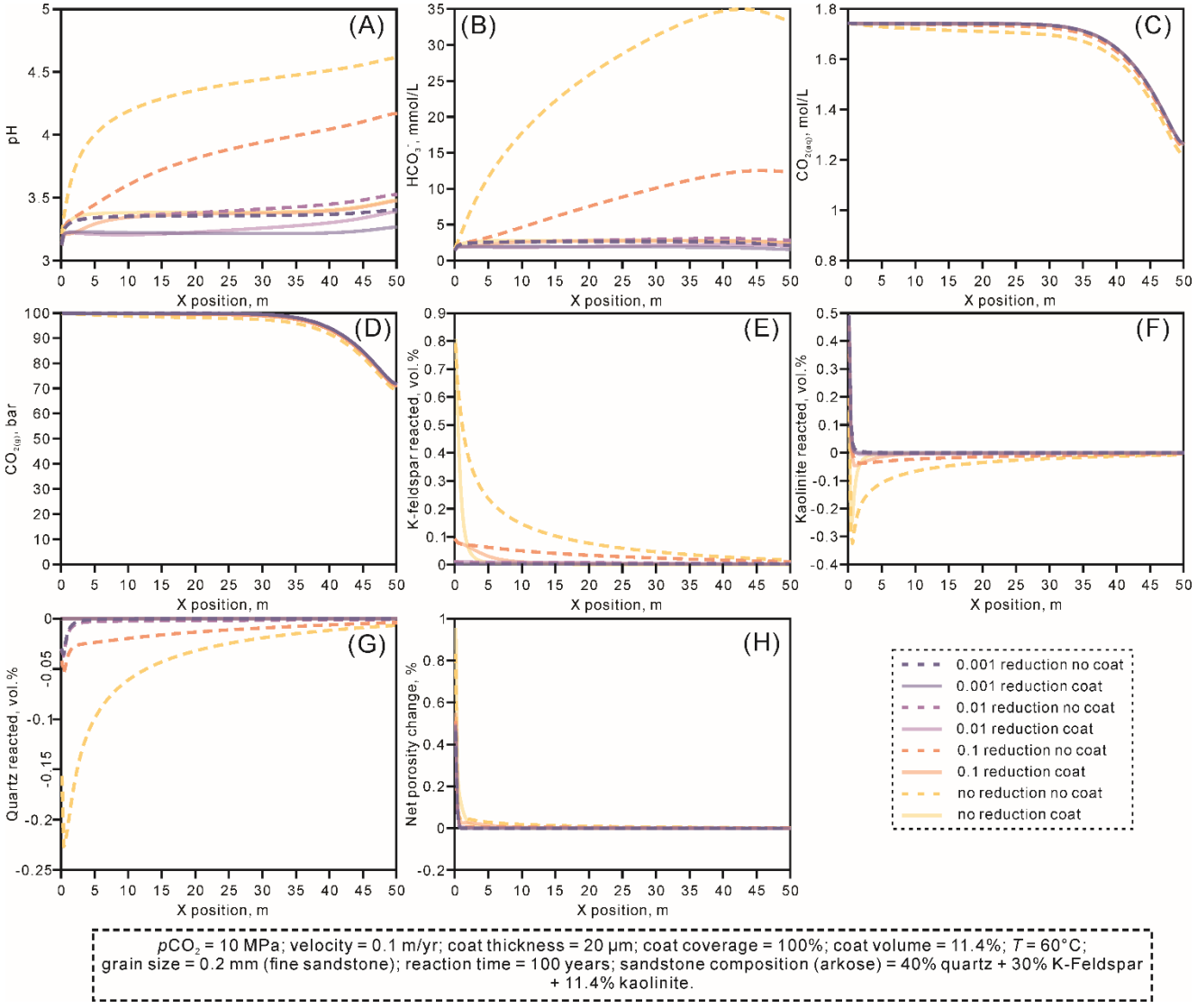

Fig. S19. Changes in water pH (A), CO_2 speciation (B–D), mineral dissolution and precipitation (E–G), and net porosity changes (H) using different orders of reduction of K-feldspar dissolution rate after the injection of CO_2 over 100 years. In panels E–G, positive values indicate mineral dissolution, while negative values indicate mineral precipitation. In the panel H, positive values indicate net porosity increase, while negative values indicate net porosity decrease. pCO_2 = partial pressure of injecting CO_2 gas.

7. Water-CO_2-rock interactions in illite-coated sandstones

7.1. Water-CO_2-rock interactions using variable illite coat parameters

7.1.1. Variable coat coverages

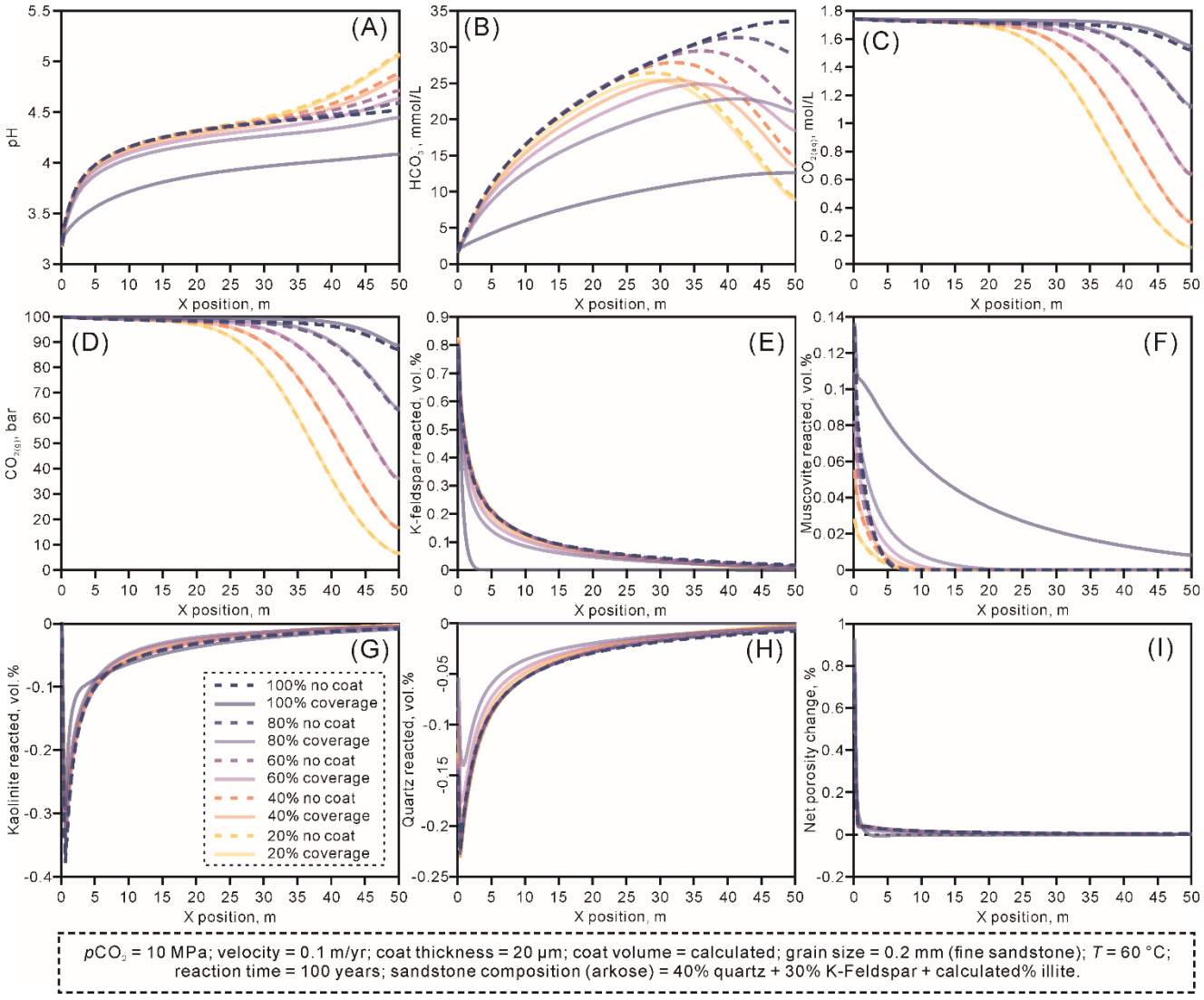

Fig. S20. Changes in water pH (A), CO_2 speciation (B–D), mineral dissolution and precipitation (E–H), and net porosity changes (I) using different coat coverages after the injection of CO_2 over 100 years. n panels E–H, positive values indicate mineral dissolution, while negative values indicate mineral precipitation. In the panel I, positive values indicate net porosity increase, while negative values indicate net porosity decrease. pCO_2 = partial pressure of injecting CO_2 gas.

7.1.2. Variable coat thicknesses

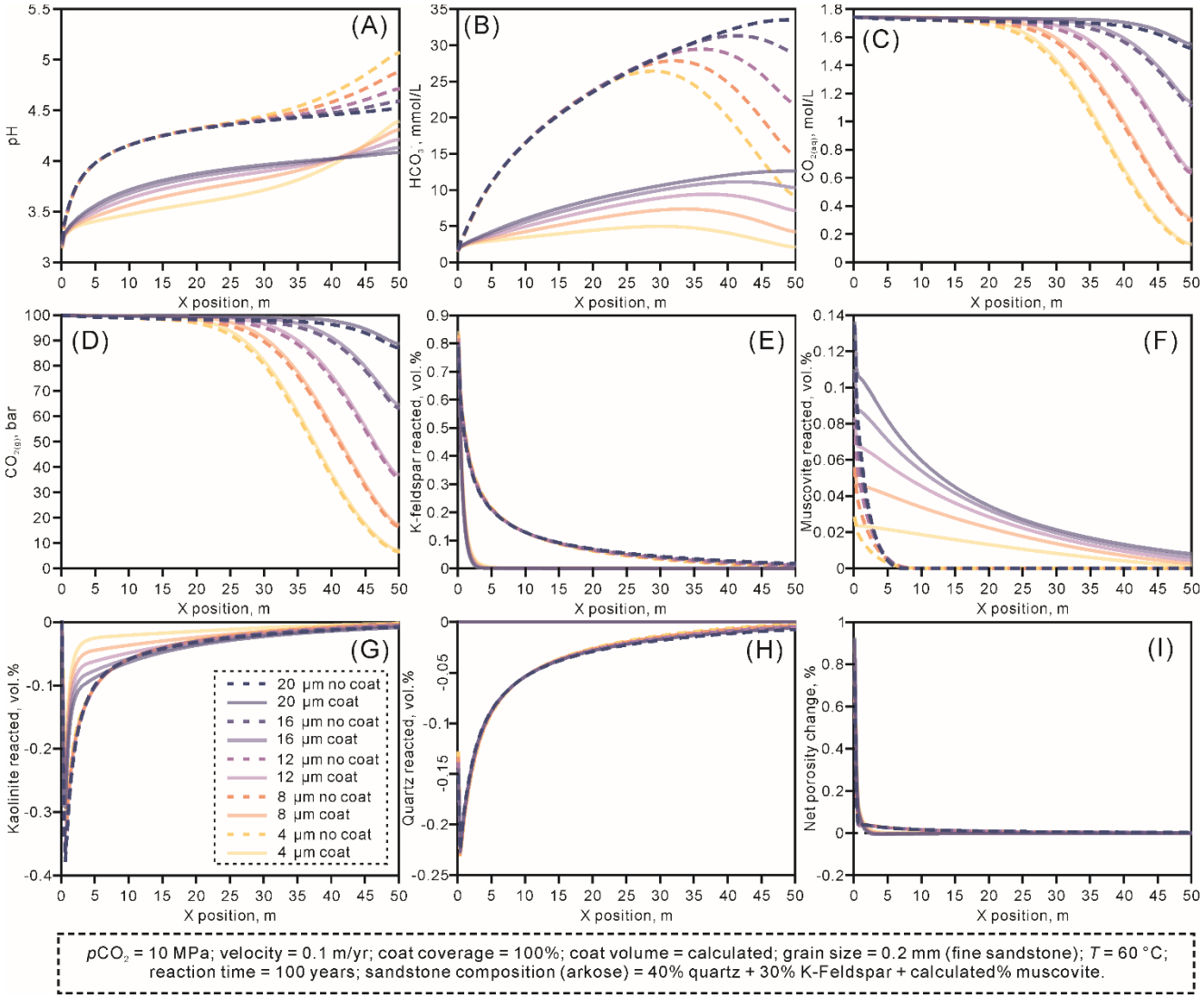

Fig. S21. Changes in water pH (A), CO_2 speciation (B–D), mineral dissolution and precipitation (E–H), and net porosity changes (I) using different coat thicknesses after the injection of CO_2 over 100 years. In panels E–H, positive values indicate mineral dissolution, while negative values indicate mineral precipitation. In the panel I, positive values indicate net porosity increase, while negative values indicate net porosity decrease. pCO_2 = partial pressure of injecting CO_2 gas.

7.2. Water-CO_2-rock interactions using variable grain sizes

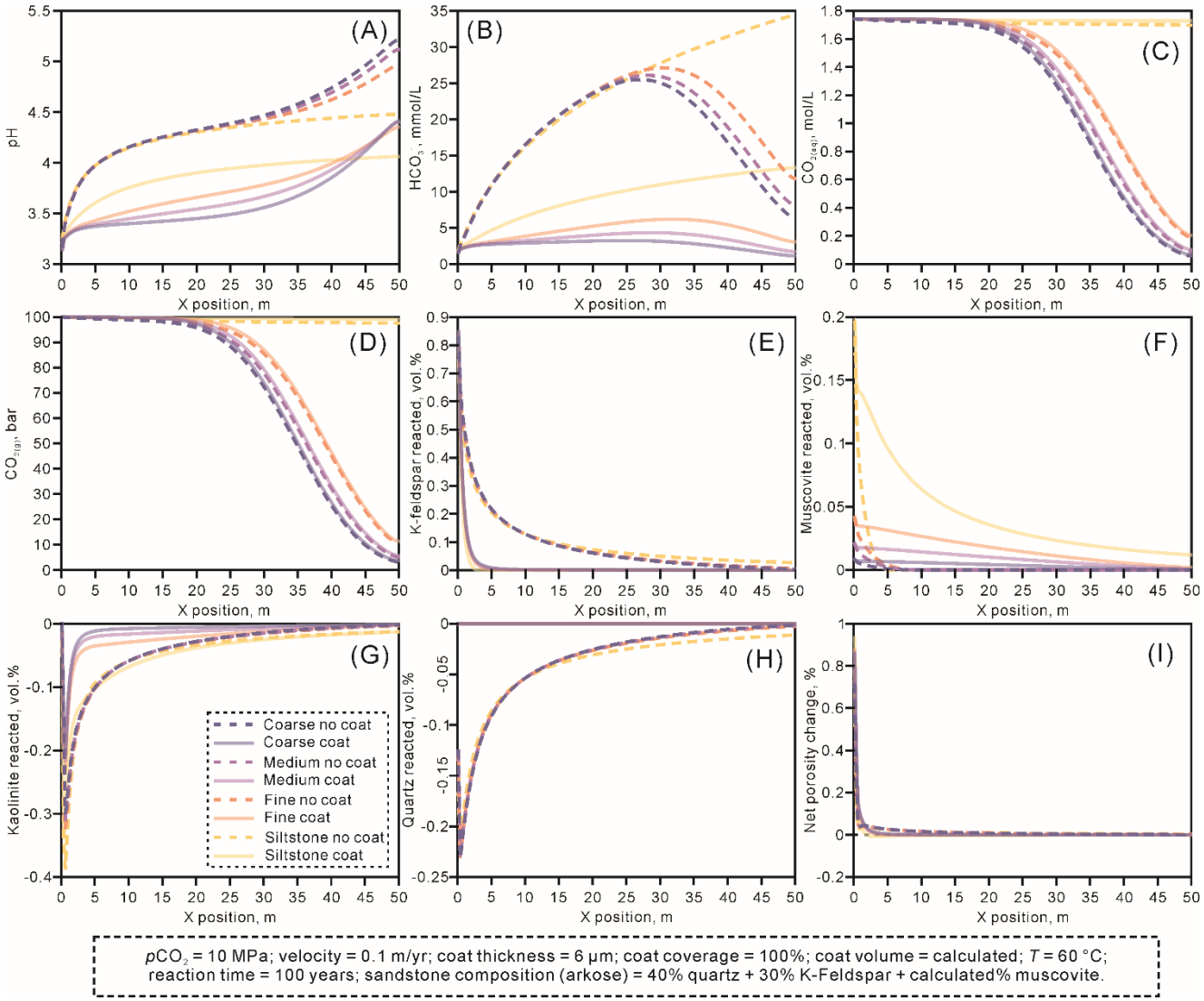

Fig. S22. Changes in water pH (A), CO_2 speciation (B–D), mineral dissolution and precipitation (E–H), and net porosity changes (I) using different detrital gain sizes after the injection of CO_2 over 100 years. In panels E–H, positive values indicate mineral dissolution, while negative values indicate mineral precipitation. In the panel I, positive values indicate net porosity increase, while negative values indicate net porosity decrease. pCO_2 = partial pressure of injecting CO_2 gas.

7.3. Water-CO_2-rock interactions using variable detrital lithologies

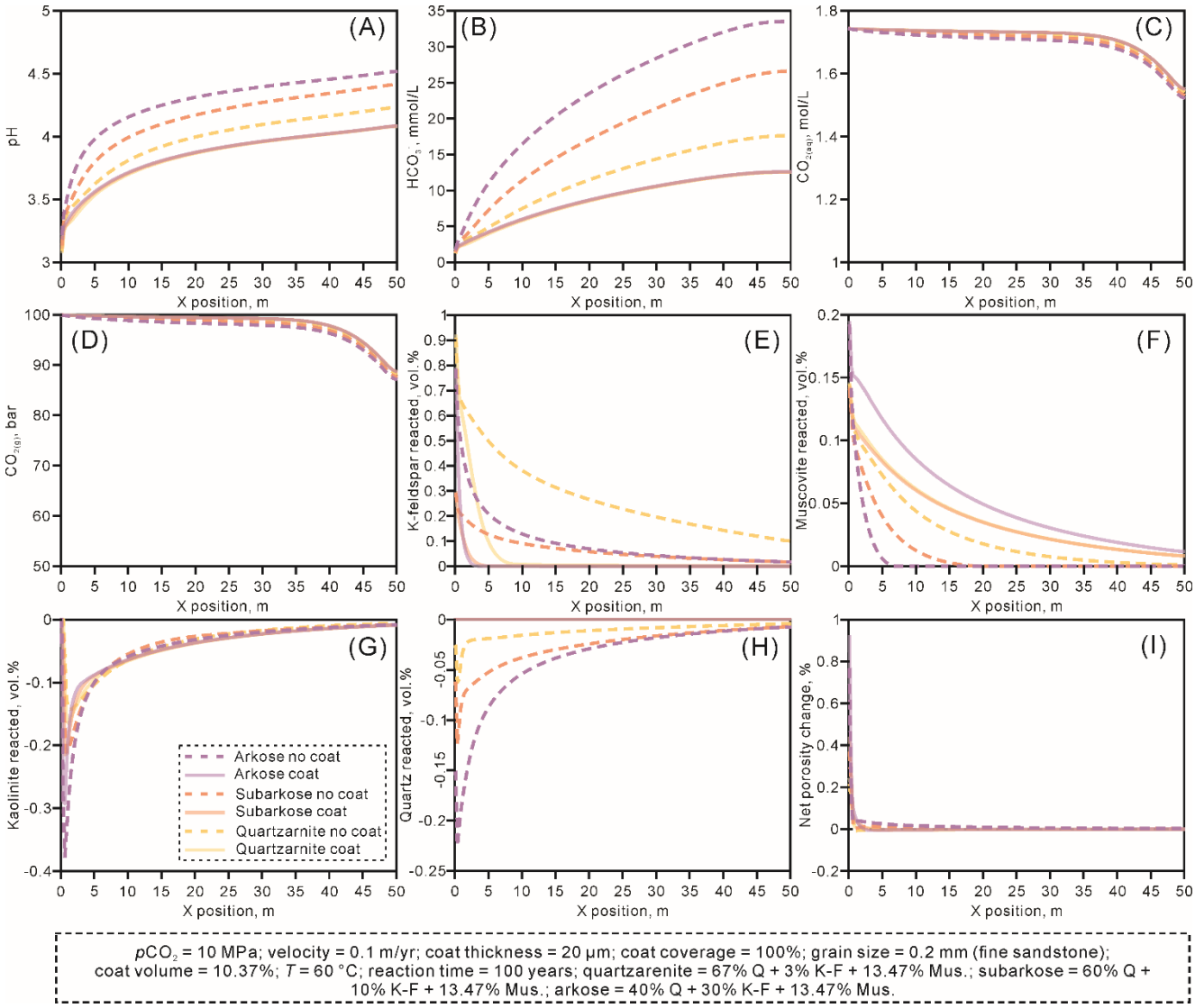

Fig. S23. Changes in water pH (A), CO_2 speciation (B–D), mineral dissolution and precipitation (E–H), and net porosity changes (I) using different detrital lithologies after the injection of CO_2 over 100 years. In panels E–H, positive values indicate mineral dissolution, while negative values indicate mineral precipitation. In the panel I, positive values indicate net porosity increase, while negative values indicate net porosity decrease. pCO_2 = partial pressure of injecting CO_2 gas.

7.4. Water-CO_2-rock interactions using variable pCO_2

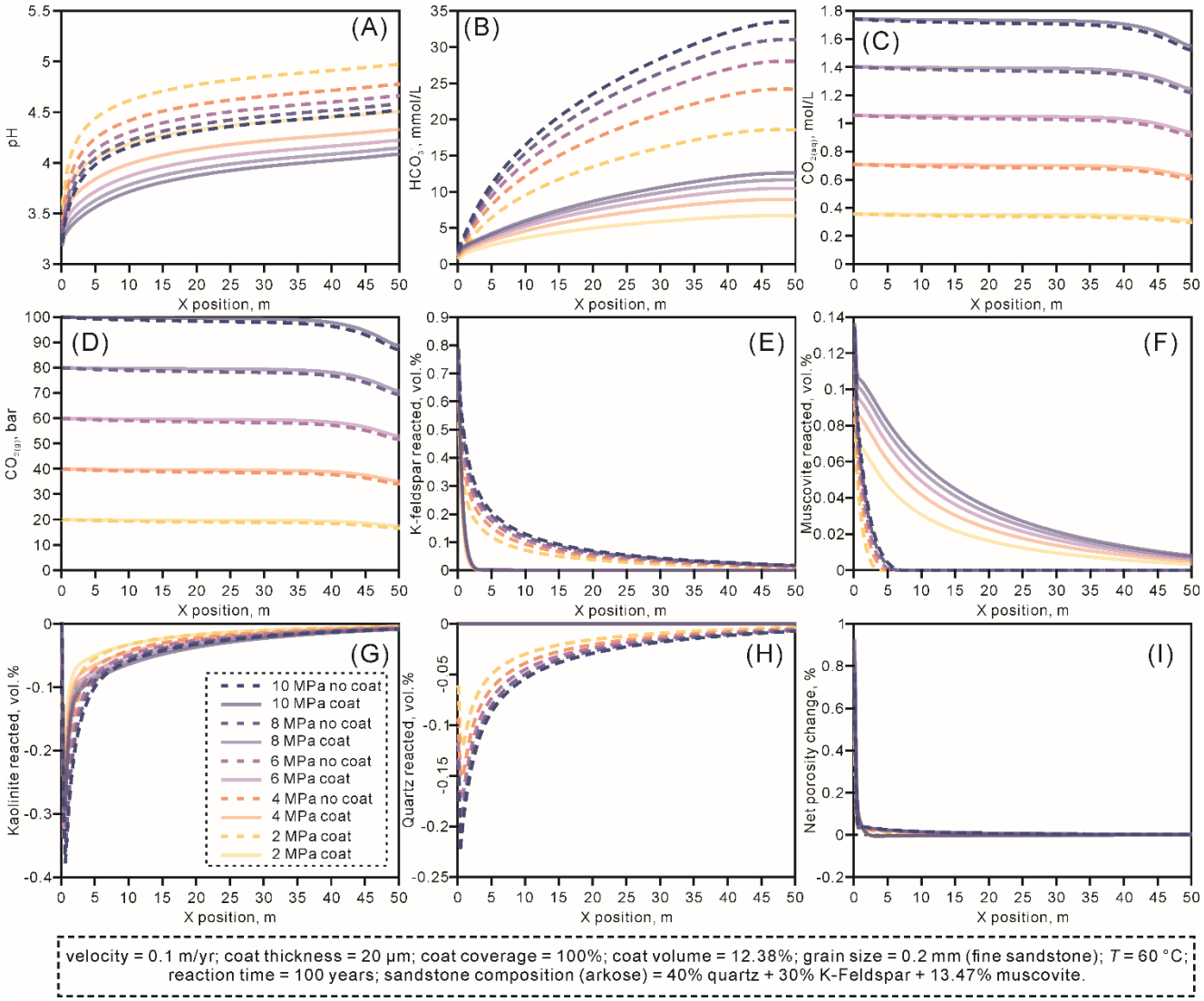

Fig. S24. Changes in water pH (A), CO_2 speciation (B–D), mineral dissolution and precipitation (E–H), and net porosity changes (I) using different partial pressures of injecting CO_2 gas (pCO_2) after the injection of CO_2 over 100 years. In panels E–H, positive values indicate mineral dissolution, while negative values indicate mineral precipitation. In the panel I, positive values indicate net porosity increase, while negative values indicate net porosity decrease.

7.5. Water-CO_2-rock interactions using variable temperatures

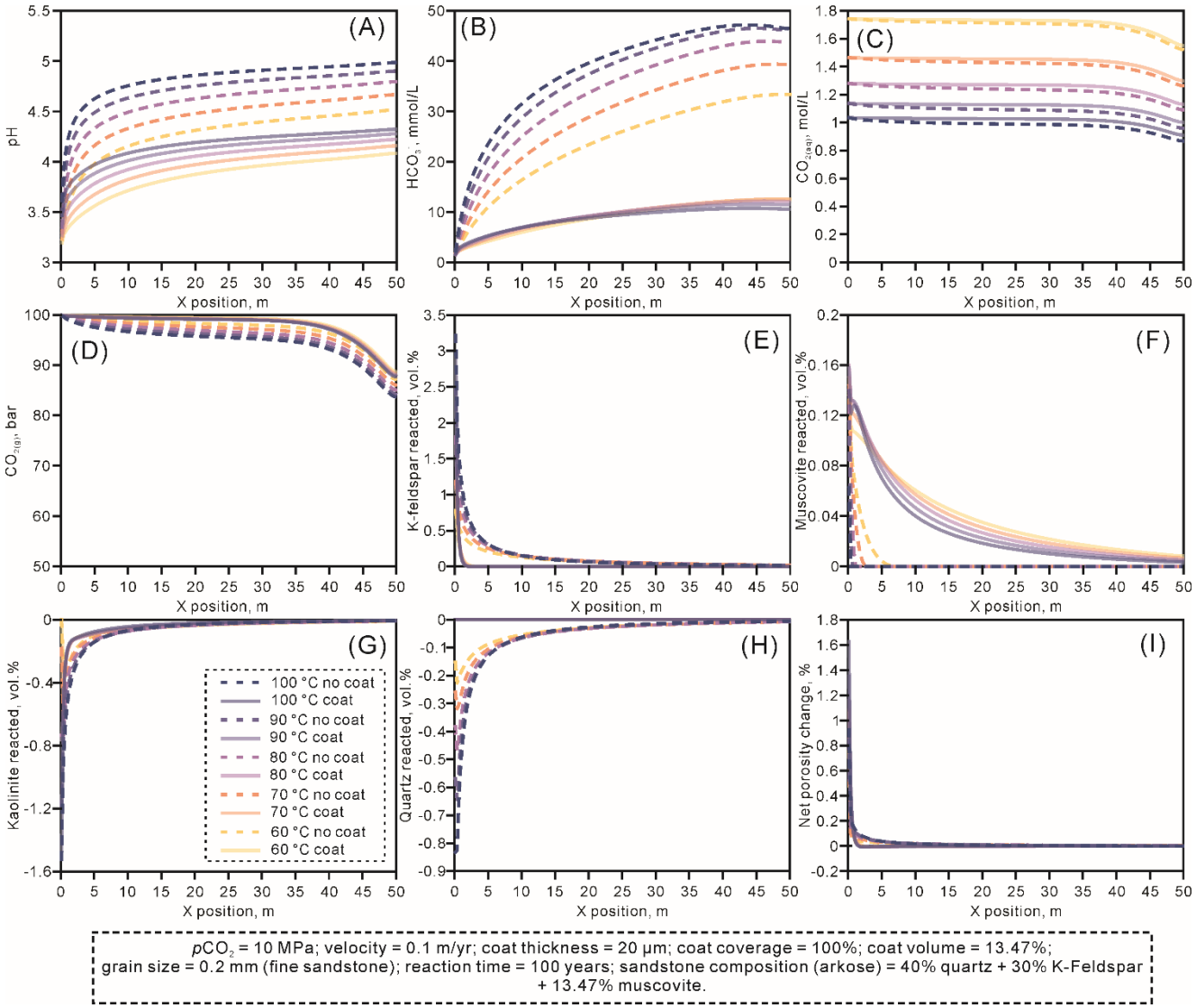

Fig. S25. Changes in water pH (A), CO_2 speciation (B–D), mineral dissolution and precipitation (E–H), and net porosity changes (I) using different temperatures after the injection of CO_2 over 100 years. In panels E–H, positive values indicate mineral dissolution, while negative values indicate mineral precipitation. In the panel I, positive values indicate net porosity increase, while negative values indicate net porosity decrease. pCO_2 = partial pressure of injecting CO_2 gas.

7.6. Water-CO_2-rock interactions using variable fluid velocities

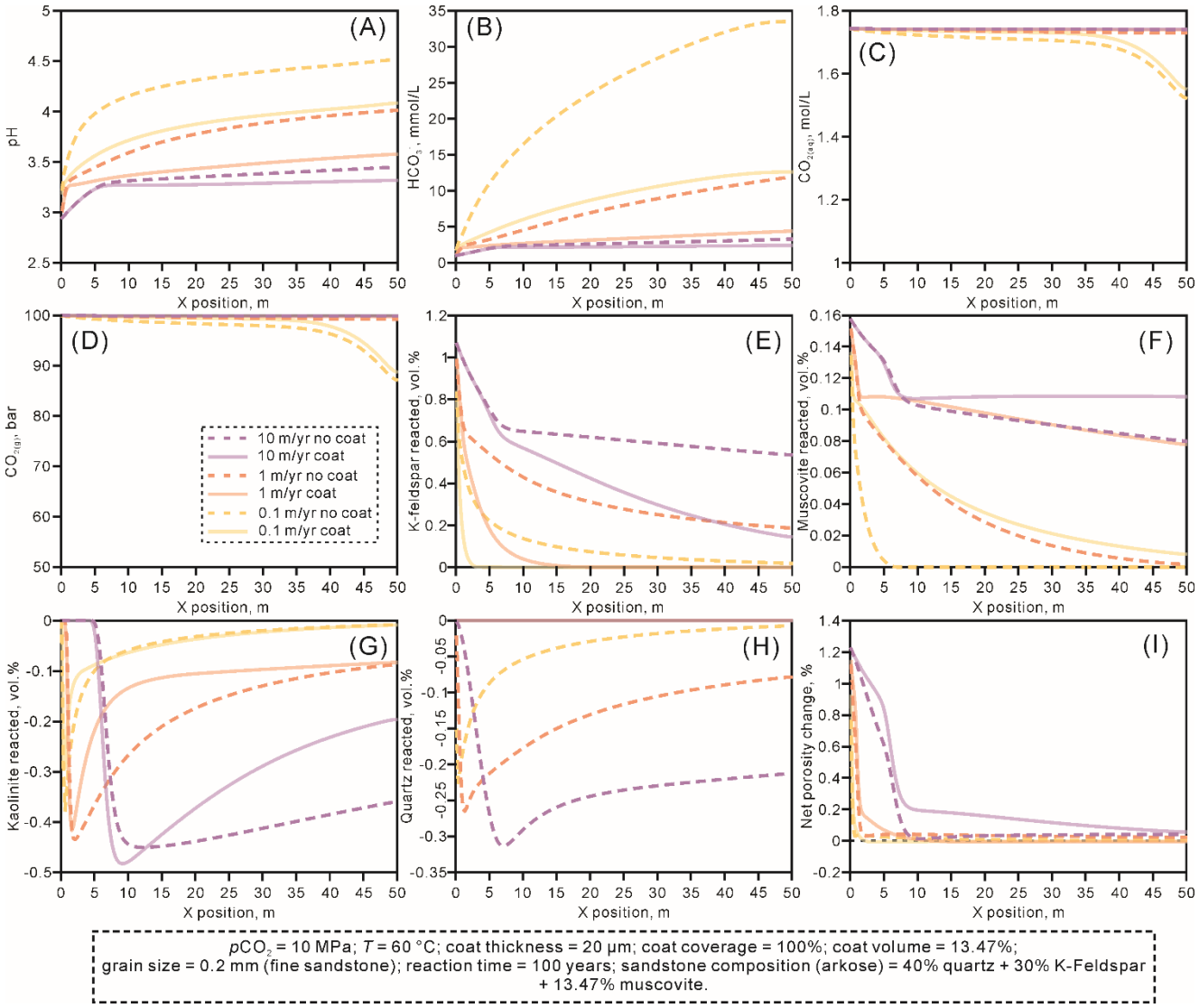

Fig. S26. Changes in water pH (A), CO_2 speciation (B–D), mineral dissolution and precipitation (E–H), and net porosity changes (I) using different fluid velocities after the injection of CO_2 over 100 years. In panels E–H, positive values indicate mineral dissolution, while negative values indicate mineral precipitation. In the panel I, positive values indicate net porosity increase, while negative values indicate net porosity decrease. pCO_2 = partial pressure of injecting CO_2 gas.

7.7. Water-CO_2-rock interactions with the incorporation of the reduction of dissolution rates of detrital grains

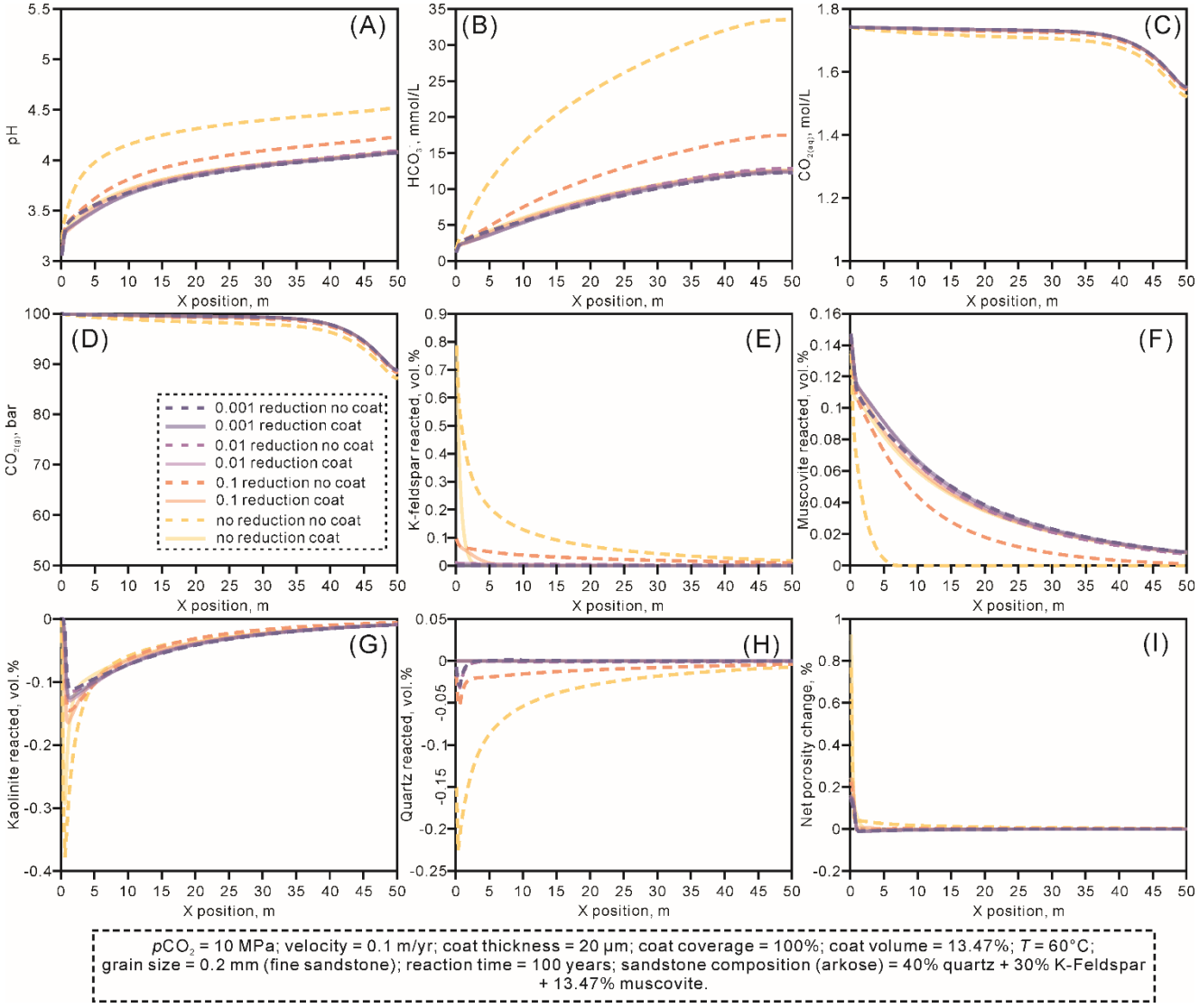

Fig. S27. Changes in water pH (A), CO_2 speciation (B–D), mineral dissolution and precipitation (E–H), and net porosity changes (I) using different orders of reduction of K-feldspar dissolution rate after the injection of CO_2 over 100 years. In panels E–H, positive values indicate mineral dissolution, while negative values indicate mineral precipitation. In the panel I, positive values indicate net porosity increase, while negative values indicate net porosity decrease. pCO_2 = partial pressure of injecting CO_2 gas.

References

Beckingham, L. E., Mitnick, E. H., Steefel, C. I., et al. Evaluation of mineral reactive surface area estimates for prediction of reactivity of a multi-mineral sediment. Geochimica et Cosmochimica Acta, 2016, 188: 310–329.

Beckingham, L. E., Steefel, C. I., Swift, A. M., et al. Evaluation of accessible mineral surface areas for improved prediction of mineral reaction rates in porous media. Geochimica et Cosmochimica Acta, 2017, 205: 31-49.

Boudreau, B. P. Diagenetic Models and Their Implementation: Modelling Transport and Reactions in Aquatic Sediments. Berlin, Springer-Verlag, 1997.

Emmanuel, S. Modeling the effect of mineral armoring on the rates of coupled dissolution-precipitation reactions: Implications for chemical weathering. Chemical Geology, 2022, 601: 120868.

Golubev, S. V., Bénézeth, P., Schott, J., et al. Siderite dissolution kinetics in acidic aqueous solutions from 25 to 100 °C and 0 to 50 atm pCO_2. Chemical Geology, 2009, 265: 13-19.

Lammers, K., Smith, M. M., Carroll, S. A. Muscovite dissolution kinetics as a function of pH at elevated temperature. Chemical Geology, 2017, 466: 149-158.

Li, H., Hu, Q., Jones, S., et al. A review and discussion on the influences of grain-coating clay minerals on water-rock interactions in sandstones. Earth-Science Reviews, 2025, 263: 105073.

Luhmann, A. J., Kong, X. Z., Tutolo, B. M., et al. Experimental dissolution of dolomite by CO_2-charged brine at 100 °C and 150 bar: Evolution of porosity, permeability, and reactive surface area. Chemical Geology, 2014, 380: 145-160.

Palandri, J. L., Kharaka, Y. K. A compilation of rate parameters of water-mineral interaction kinetics for application to geochemical modelling, Menlo Park, Geological Survey, 2004.

Park, A. J. Water-rock interaction and reactive-transport modelling using elemental mass-balance approach: I. The methodology. American Journal of Science, 2014, 314: 785-804.

Pokrovsky, O. S., Golubev, S. V., Schott, J., et al.Calcite, dolomite and magnesite dissolution kinetics in aqueous solutions at acid to circumneutral pH, 25 to 150 °C and 1 to 55 atm pCO_2: New constraints on CO_2 sequestration in sedimentary basins. Chemical Geology, 2009, 265: 20-32.

Schulz, H. D., Zabel, M. Marine Geochemistry. Berlin, Heidelberg, Springer-Verlag, 2006.